NTNU

Norwegian University of
Science and Technology

Hybrid HVDC Transmission for Large-Scale Offshore Wind Integration

Model-Based Control Design and
Performance Assessment

Inga Haukaas

Master of Energy and Environmental Engineering
Submission date: June 2017
Supervisor: Olimpo Anaya-Lara, IEL
Co-supervisor: Raymundo E. Torres-Olguin, SINTEF

Norwegian University of Science and Technology
Department of Electric Power Engineering

Abstract

Today, the world faces major challenges regarding our global environment. The most pressing challenge is global warming, and the scientific community is well aware of the catastrophic consequences an increase in global temperature will have. There is a global understanding that fossil fuels must be phased out as soon as possible, and renewable energy sources must replace them. Wind power is an important energy source which is mostly exploited onshore. Today, the number of offshore wind farms is increasing because they have some advantages over onshore installations like the high wind speeds and low turbulence. A challenge for offshore wind farm developers, are the transportation of power over long distances. HVDC-transmission technology is the preferred solution for offshore transportation, but it is dependent on an offshore converter station. It is expensive to install the converter station at deep water, therefore possible solutions for reducing the cost must be investigated.

This Master's thesis has investigated a hybrid converter topology which will reduce the power losses and the cost. The hybrid converter consists of a diode rectifier connected in series with a voltage source converter. The two converters complement each other in a way such that the power losses and the total cost are kept low. The hybrid solution has few active power devices and will therefore be a reliable and robust converter station. A model-based controller for the hybrid converter was proposed. The controller makes the solution flexible and adaptable to the system dynamics. The hybrid topology was compared with other converter topologies to see the benefits of using the hybrid solution.

The work on the hybrid converter began by reviewing proposals on alternative solutions for the converter platform. The control theory was studied to create a foundation of knowledge for the control design. The control objectives for the system was determined in the beginning because the objectives decide which parameters are to be controlled. Several control objectives makes the controller more complex and difficult to implement. A model-based controller was developed by utilizing a procedure from the passivity-based control theory. A model of the system was implemented in the simulation program PSCAD/EMTDC and the control system was simulated.

Several approaches for the control design were tested before a final solution for a system with two control objectives was found. A dynamic performance assessment was performed on the final controller to validate that it performed well. A comparison between the different solutions showed that the hybrid topology has the advantages of lower losses and total cost. The hybrid topology showed promising results for further research and a detailed plan for future work was given in this thesis.

Sammendrag

I dag står verden overfor store utfordringer angående vårt globale miljø og den viktigste utfordringen er global oppvarming. Det vitenskapelige samfunnet er klar over de katastrofale konsekvensene en økning i global temperatur vil ha, og det er en global forståelse for at fossilt brensel må fases ut. Fornybare energikilder slik som vind, sol og vann må erstatte de forurensende energikildene. Vindkraft er en viktig energikilde som hovedsakelig utnyttes på land. Havmølleparker øker i antall i dag fordi de har noen fordeler overfor landanlegg, som for eksempel de høye vindhastighetene og at det er store områder som kan utnyttes. En utfordring med havmølleparker er transport av kraft over lange avstander med vanskelig vær. HVDC-overføringsteknologien er den foretrukne løsningen for transport av strøm til sjøs, men den er avhengig av en omformerstasjon. Det er dyrt å installere omformerstasjoner i dypt vann, derfor må mulige løsninger som kan redusere kostnadene undersøkes.

Denne masteroppgaven har undersøkt en hybrid omformer topologi som vil redusere tap og kostnader. En modellbasert regulator har blitt designet for den hybride løsningen som består av en diode-likeretter koblet i serie med en spenningskildeomformer. De to omformerne utfyller hverandre på en måte slik at tapene og kostnadene holdes lave. Hybridløsningen har få aktive brytere som resulterer i en pålitelig og robust konverteringsstasjon, og regulatoren gjør den fleksibel og tilpassingsdyktig i systemet. Fordelene med hybridløsningen har blitt sammenlignet med andre omformerstasjoner.

Arbeidet med hybridomformeren begynte ved å undersøke alternative løsninger for konverteringsplattformen. Kontrollteorien ble studert for å skape et grunnlag for kunnskap innen regulatordesign. Målene til systemregulatoren ble bestemt i begynnelsen før regulatoren ble designet. Grunnen var at målene bestemmer hvilke av parameterne som må kontrolleres, og hvor komplisert regulatoren blir. En modellbasert regulator ble utviklet ved å benytte en prosedyre fra den passivitetsbaserte kontrollteorien. En modell av systemet ble implementert i simuleringsprogrammet PSCAD / EMTDC og kontrollsystemet ble simulert.

Flere tilnærminger til kontrolldesign ble testet før en endelig løsning for et forenklet system ble funnet. En dynamisk ytelsesvurdering ble utført på den endelige regulatoren for å validere at den fungerte bra. En sammenligning mellom ulike løsninger viste at hybridtopologien har fordelene av færre tap og lavere kostnader. Hybridtopologien viste lovende resultater for videre forskning, og til slutt i oppgaven er det gitt en detaljert plan for fremtidig arbeid.

Preface

This Master's thesis is the result of my final semester as a master student at the Department of Electrical Engineering, Norwegian University of Science and Technology (NTNU). The work was carried out during the spring of 2017, as a continuation of my specialization project titled "*HVDC-connection of Large Offshore Wind Farms Using a Low-Cost Hybrid Converter*".

The main motivation for choosing this topic for my specialization project and Master's thesis is because I see a lot of potential in offshore wind development. Transportation of offshore wind power is a great challenge in the energy sector today and the work of this thesis has also been a great challenge. I like to push myself towards challenging goals which motivate me to work hard. This thesis has been very challenging and given me a lot of work and frustration, but people around me have encouraged me to continue the work. Especially my mentor and co-supervisor, Dr. Raymundo Torres-Olguin has been there every day to motivate me through difficulties. I owe him my sincere gratitude for the countless hours he has spent working with me on my thesis. I know he will be a great supervisor for a lucky student one day.

I would like to convey my sincere gratitude to Prof. Olimpo Anaya-Lara, my supervisor. He has given me the great opportunity to work on an interesting topic which is very relevant in research today. He has the ability to explain difficult subjects in an easy way, which has helped me a lot in the search for more knowledge. I have learned so much from him this past year and he has motivated me to challenge myself further and to work hard. I would also like to thank him for the many hours he has spent on my thesis. Another person who deserves my heartfelt gratitude is my boyfriend, Snorre Jablonski, who has always given me his support. He also offered his brilliant English skills in the final correction of the thesis and made the last days more relaxed.

Trondheim, June 22, 2017

Inga Haukaas

Contents

List of Figures

List of Tables

Acronyms

12P-DR	Twelve pulse diode rectifier
2L-VSC	Two level voltage source converter
6P-DR	Six pulse diode rectifier
ac	Alternating current
APF	Active power filter
AS	Ancillary Services
BPF	Bandpass filter
dc	Direct current
DR	Diode rectifier
ESDI	Energy shaping plus damping injection
FRC	Fully Rated Converter
FRC-WF	Fully rated converter wind farm
GSVSC	Grid side voltage source converter
HVAC	High-voltage alternating current
HVDC	High-voltage direct current
IGBT	Insulated gate bipolar transistor
KCL	Kirchhoff's current law
KVL	Kirchhoff's voltage law
LCC	Line-commutated converter
LTI	Linear time-invariant
OWF	Offshore wind farm
PBC	Passivity-based control
PCC	Point of common coupling
PI controller	Proportional plus integral controller
PLL	Phase locked loop
PWM	Pulse width modulation
RES	Renewable energy sources
THD	Total harmonic distortion
VSC	Voltage source converter

WF Wind farm

WFVSC Wind farm voltage source converter

WPP Wind power production

WT Wind turbine

Chapter 1

Introduction

1.1 Background and Motivation

Renewable Energy and Offshore Wind Developments

One of the main global challenges of our time is how the increase in global temperature can be prevented. Most climate experts agree that global warming will result in more extreme weather, extinction of several species, melting ice in Greenland and in the Arctic which will cause a rise in sea level and weaken the Gulf Stream [1]. It is commonly known that global warming is a consequence of carbon pollution among other greenhouse gases. An important step in the right direction is the Paris agreement that entered into force in November 2016. It obligates governments to take actions on limiting the global temperature increase to two degrees [2]. One of the actions that must be fulfilled to achieve the two-degrees target, is to replace conventional power plants based on fossil fuels with renewable energy sources (RES). This is probably the greatest challenge in the energy sector today.

Wind power is a RES with a lot of potential both onshore and offshore. In the EU, during 2015, wind power production (WPP) had the highest share of financial investments among all the RES [3]. Several factors underpin the increasing investment in offshore wind farms (OWFs), e.g. the lack of space limitations, high wind speeds, and little turbulence. However, there are many challenges with OWFs and this thesis will focus on a technical solution

which can improve the efficiency of the power transfer.

High-voltage direct current (HVDC) transmission is preferred over high-voltage alternating current (HVAC) for OWF connections. A major drawback with HVAC is the fact that ac transmission over large distances requires reactive power compensation, thus less active power can be transmitted. HVDC transmission does not require reactive power compensation and will thus have smaller losses and the cost will be lower for large distances [4]. HVDC installations are more expencive than HVAC, thus the break-even distance in Fig. 1.1 illustrates when HVDC transmission is more profitable than HVAC, and the distance is around 100-150 km [5].

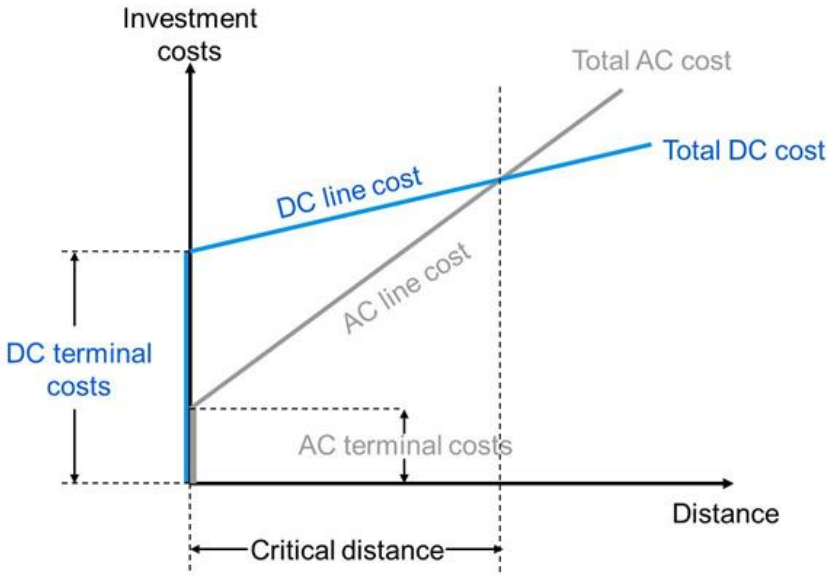

Figure 1.1: Total cost of HVDC and HVAC transmission illustrating the break even distance, [6].

HVDC Technology

There are two main HVDC technologies; line-commutated converters (LCCs) and voltage source converters (VSCs). LCC, also called classic HVDC, is the traditional technology which has some drawbacks compared to VSC technology. The valves in the LCC are built with thyristors and need a strong ac network to operate. A large amount of reactive power is drawn from the grid and low-order harmonics are introduced because of the low-frequency commutation process [7]. Capacitors are needed for reactive power support and reactors to filter harmonics. The need for huge passive elements results in a large footprint, i.e. space

needed on the offshore platform. Installation of a large offshore platform is an important engineering challenge, which is why an LCC is undesirable in for OWFs.

The VSC technology utilizes transistors which can be turned on and off and it was introduced in the 1990's [7]. The VSC has the advantage of utilizing fully controlled power devices, compared to an LCC which utilizes thyristors that can only be turned on. VSCs are self-commutating because they are fully controllable, and this makes them less dependent on a strong ac network. The VSC can be switched at high frequency (kHz) because it is not dependent on a strong ac grid, which the LCC is. The converter will produce a smaller amount of harmonic pollution by increasing the switching frequency, which results in smaller filters. Moreover, the VSC has full control over reactive and active power, thus there is no need for reactive power compensation [7]. A drawback of using VSCs is the high switching frequency which results in high switching losses. This is the reason why VSCs normally are used where there is a need for black start capability or lack of space, which is the case for OWFs. The comparison of LCCs and VSCs are summarized in Table 1.1.

Table 1.1: Comparison table between an LCC and a VSC

	LCC	**VSC**
Grid support capability	No	Yes
Footprint	Large	Small
Losses	Low	Higher
Black start capability	No	Yes

The motivation for this thesis is the fact that there is still a possibility to improve the HVDC technology for OWFs. Some main factors which must be improved are:

- The space required for the converter platform at deep sea should be limited because of the challenges related to the installation of platforms.
- The platform should also be robust, such that it can handle rough sea and weather.
- Another important factor is the losses connected to the transportation of power over long distances, which must be reduced to reduce the total cost.

1.2 Objectives

The main objectives of this thesis are:

1. Investigate and compare different converter configurations for offshore integration.
2. Investigate a hybrid solution for a converter planned to be installed on an offshore platform which can reduce the total cost.
3. Design a control system for the hybrid converter station in the stationary reference frame.
4. Investigate the control system behavior and the system dynamic performance.

1.3 Methodology

- A literature review on alternative solutions for the converter platform was performed.
- A model-based controller was designed based on the system equations in the stationary reference frame.
- The proposed controller was validated in an electromagnetic transient simulation program called PSCAD/EMTDC.

Modeling Assumptions and Simulation Remarks

- A detailed switching model was used.
- The VSC was implemented as a two-level converter, where one switch represents several switches connected in series.
- The OWF was represented as an ideal voltage source for simplifications. It was assumed that the ac voltage was controlled by the OWF.
- The transformer connected to the VSC was neglected to simplify the model further.

1.4 Contribution of Master Thesis

This Master thesis investigates a hybrid converter topology which will reduce the power losses and the cost. The advantages of the hybrid topology are compared with two other converter configurations that aim to reduce the cost of the offshore converter station. Model-based controllers for the hybrid topology are designed and tested. The three converter solutions compared in the report are:

1. **A diode-based HVDC link** utilizing uncontrollable diode rectifiers (DRs) have been proposed by Blasco et al. in [8], [9], [10]. The topology in [9] takes advantage of the modern wind turbine (WT) technology by utilizing synchronous generators connected through a back-to-back converter. The fully-rated converter wind farm (FRC-WF) has a tight control of the terminal voltage, such that the uncontrolled DR can be utilized for power conversion. The advantages of this system are lower losses and costs while keeping a high reliability. However, the DR creates harmonic pollution, and therefore a large filter bank is needed to eliminate the disturbances.

2. **The diode-based HVDC link with an active power filter (APF)** is a possible solution which can improve the topology proposed by Blasco et al. APFs are not common in high power systems (>10 MVA) but they can provide both harmonic- and reactive power compensation, such that bulky passive filter banks and capacitors will not be necessary. The APF is smaller than the passive filter banks, such that the size of the converter platform will be reduced and thus the total cost decreases. There are no APF installations in the offshore power grid today, but this is an area where APFs can provide some advantages in the future. The railway power line is one area where APFs are installed in high power grids today and in [11], several shunt APF in a range of 40 MVA to 60 MVA have been installed in substations along the Tokaido Shinkansen. This is an example that APFs are successfully installed in high power grids today, which means that it can be installed in the offshore power grid in the future.

3. **A hybrid DR-VSC topology** is a novel topology proposed by Nguyen et al. in [12] and [13]. This solution consists of a 12-pulse DR (12P-DR) and a VSC connected in series on the offshore converter platform. The two converters complement each other in a way such that the power losses and total cost are kept low. The hybrid converter

has few active elements which reduce the losses and make it reliable and robust. The converter is also controllable which makes it flexible and adaptable to the system dynamics. The simulation results shown in [12] are promising for further research on the hybrid topology, and an alternative controller will be designed and tested in this thesis.

1.5 Thesis Outline

The thesis consists of six chapters organized as follows:

Chapter 1 presents the converter topologies which are compared in this thesis and the main motivation for the work. The objectives and methodology are described.

Chapter 2 introduces some of the challenges with OWF integration and gives an introduction to the topology of the different converters presented in this thesis. Also, some important system components are described.

Chapter 3 explains the control objectives of the different solutions and important aspects of control theory which are relevant to this thesis.

Chapter 4 explains the controller of the active power filter and shows some simulation results.

Chapter 5 shows the development of the controller for the hybrid converter and discusses the simulation results.

Chapter 6 compares the three converter configurations and draws some main conclusions. Finally, some possible future work is listed.

Chapter 2

Offshore Wind Farm Integration using HVDC

2.1 Introduction

It was stated in the Global Wind Report from 2016 [14], that for some circumstances the offshore wind energy is cheaper than onshore. This is one of the reasons why development of OWFs is increasing, as can be seen in Fig. 2.1. To continue this path, it will be necessary to move some of the development from shallow to deep water. The advantages of developing WFs in deep water are for instance:

- the vast space,
- the great wind resource,
- the reduction of visual impact and noise.

On the other hand, major drawbacks with deep water installations are the high cost of power transmission and platform installations.

Integration solutions for offshore wind farms (OWFs) are important research areas today. By finding new solutions, it will be possible to reduce the total cost of OWF integration and thus more RES can replace fossil fuels. One of the objectives of this thesis is to investigate a hybrid solution for an offshore converter station in deep water, which can reduce the cost of the platform. In modern applications, the VSC-based HVDC topology has become more

common, but it needs expensive switching components and has high switching losses. Thus, it will be beneficial to investigate new solutions that can reduce both cost and losses.

Three converter platform solutions were introduced in the previous chapter, and a more detailed explanation of the system typologies will be given in this chapter. Important issues that the system must handle will be introduced and components of the offshore system will be presented.

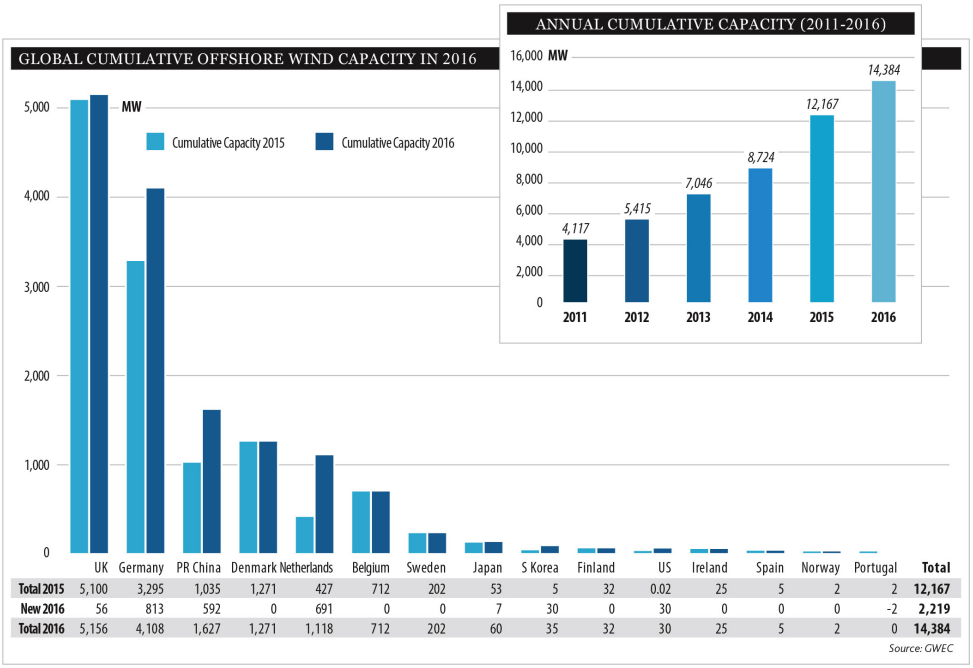

Figure 2.1: Annual cumulative offshore wind capacity from 2011 to 2016, and offshore wind capacity for different countries in 2015 and 2016 [14].

2.2 Grid Connection Codes

The increasing share of WPP will have a great impact on the power system operation. The WPP will replace the conventional power plants which are based on fossil fuels and easy to control. OWFs are difficult to control and unpredictable, and this will have a great impact on the security of supply.

To maintain power system security and improve system stability, it will be necessary for the wind farms (WFs) to provide some Ancillary Services (AS) to the same extent as conventional power plants. The AS are described in the Grid Codes of each respective country, and the Grid Codes provided by ENTSO-E [15] are an attempt to create common

Grid Codes in Europe. The Grid Codes specify the requirements that are mandatory for connection of generation or loads to the electrical network, and the requirements ensure efficient power transmission and a safe and economic power system [16]. One AS which the WF must be able to provide is e.g. reactive power support. This service will keep the power factor at connection point close to 1 and make sure maximum active power is delivered from the WF to the load. It is important that reactive power in the offshore ac grid is compensated, such that maximum power will be transported to shore.

Another AS which is especially important for providing system stability is frequency support. The frequency is a stability measure which indicates if the consumption exceeds the production with a drop in frequency and vice versa. It is stated in the Grid Codes that generation plants need to deliver frequency support as an AS if the frequency drop exceeds the statutory limits [17]. The next section will explain an important issue which is also discussed in the Grid Codes.

2.3 Power Electronic Interfaces

Power electronics like the DRs are a source of harmonics because they are not controllable [18]. Harmonics distort the voltage or current waveform because they contain components at harmonic frequencies (multiples of the system frequency). The DRs are preferred in cases where the power flow is unidirectional, and especially if the power level is high. This is because the power losses are smaller than in converters based on switching devices, thus the DRs are cheaper and more robust. But the drawback of DRs is the harmonic distortion which causes losses and influences the quality of voltage supply [17]. The diode-based HVDC link topology proposed by Blasco et al. [9] takes advantage of the fact that the DR has lower losses in high power levels than a VSC-based HVDC link. The disadvantage of the topology is, as mentioned before, the need for passive filters to eliminate the harmonic voltage components. The passive filters consist of tuned L-C components which are both efficient and has a low cost [11]. However, there are disadvantages of the passive filters such as the large size, mistuning, and resonance with load and impedances. Because of these drawbacks, the APFs have become an alternative to the passive filters as described for the alternative solution to the diode-based HVDC link. More details on the active power filter

will be given in Ch. 4.

The total harmonic distortion (THD) in the voltage or current waveform is quantified to be used as an indicator of the quality of the system voltage or current. The index is given in percentage and calculated for the source current i_s as [18]:

$$\%THD_i = 100\sqrt{\sum_{h\neq 1}\left(\frac{I_{sh}}{I_{s1}}\right)^2}$$

where the capital letter I_s represents the RMS value of the source current, the subscript h stands for harmonic component and subscript i indicates the THD in the current. A similar index THD_v can be calculated by using voltage components in the same equation.

2.4 System Topologies Investigated

2.4.1 Diode-Based HVDC link

The configuration of the diode-based converter platform proposed by Blasco et al. [9] is shown in Fig. 2.2. Two 6P-DRs are connected in series, and connected to the offshore ac grid through a filtering transformer T_R. This topology creates a 12P-DR which will reduce the THD of the ac current. The harmonic current components which are introduced by the 12P-DR are eliminated by passive filters, and the reactive power consumed by the 12P-DR is compensated by a capacitor. The WF is connected to the converter platform through a back-to-back converter, i.e. FRC-WF and a transformer T_W. The 12P-DR are connected to dc capacitors and dc cables which are connected to the onshore converter platform.

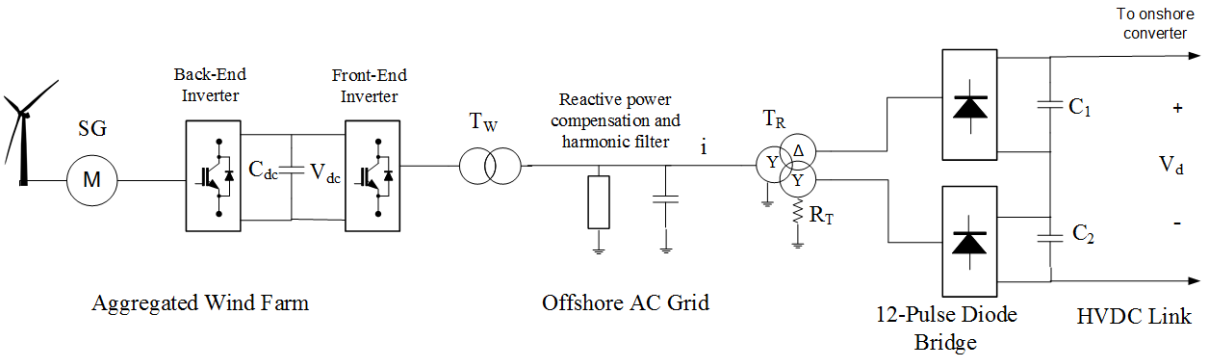

Figure 2.2: Diode-based converter platform [9].

The benefits of the DR HVDC configuration are the fact that there are no switching losses, which will improve the efficiency of the converter station compared to a VSC-based converter station. The converter will also be quite robust because there are no sensitive switching components which can easily be affected by the rough sea. Also, the cost of the platform will reduce because no expensive transistors are needed. But the drawback of this topology is the large footprint related to the bulky filters. The size of the converter platform will increase the cost of offshore installation because it is an important engineering challenge to install platforms at deep sea.

2.4.2 APF-DR Topology

The configuration of the solution utilizing an APF in the offshore ac grid is similar to the previous DR-VSC solution. Fig. 2.3 shows that the only difference in the topology is that an APF has replaced the bulky harmonic filter banks and capacitors. The APF is more compact, such that the size of the offshore converter station can be reduced. The switching devices utilized in the APF is quite sensitive and expensive, while the passive filters are more robust and cheap. However, the APF-DR solution is quite flexible in terms of harmonic compensation, which is why it is a favorable solution.

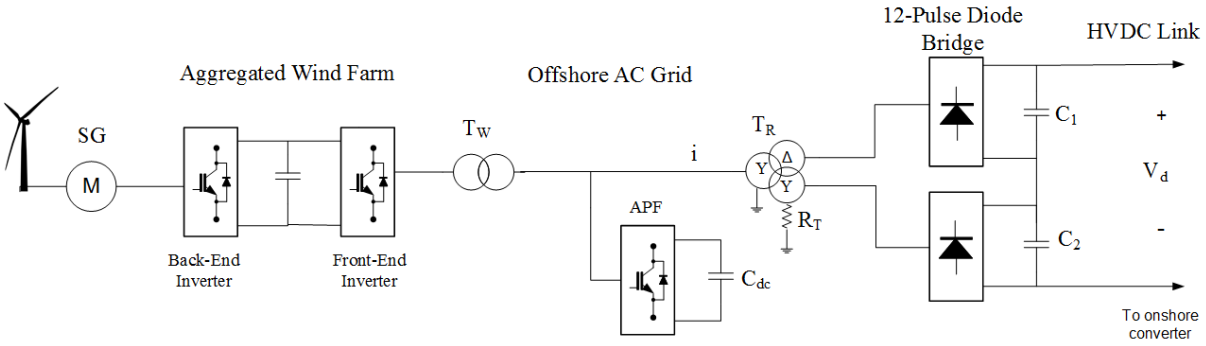

Figure 2.3: Diode-based converter platform with APF.

2.4.3 Hybrid DR-VSC Topology

One of the objectives of this thesis is to investigate a possible hybrid solution for connection of an OWF which can reduce the total cost. The solution is based on the hybrid topology presented by Nguyen et al. in [12]. Fig. 2.4 shows the hybrid topology for an HVDC link in a single line diagram. A 12P-DR is connected in series with a VSC to reduce the power rating of the VSC, and thus the considerable switching losses related to it.

The 12P-DR is connected to the ac grid through a three-winding transformer, T_{DR}, and the inductance, L_r, which works as a series filter for high-order harmonics. Capacitor C_{PCC} at the point of common coupling (PCC) is a simple shunt filter that reduces the harmonic ripples and helps to control the ac voltage. The wind farm VSC (WFVSC) is connected to the ac grid through an inductance, L_c, and a transformer, T_{VSC}, with a Y/Δ connection.

On the dc side, the 12P-DR and the WFVSC are connected to capacitors, C_1, C_2 and C_{dc}, and two dc submarine cables connect the offshore platform to shore. The grid side VSC (GSVSC) is connected to a capacitor C_d on dc side and an inductor L_g on ac side. An ideal ac grid represents the onshore network and is connected to a transformer. The dc link is built as a symmetrical monopole to avoid an offset of the ac voltage, which will create an asymmetrical voltage. An asymmetrical voltage will lead to saturation of the transformer and it must be avoided. The symmetric monopole has two poles of different polarity, but there is no grounding as in the bipolar configuration. An advantage of the symmetrical monopole is that there will not be a dc ground current, but a disadvantage compared to the bipolar configuration is the limited redundancy [19].

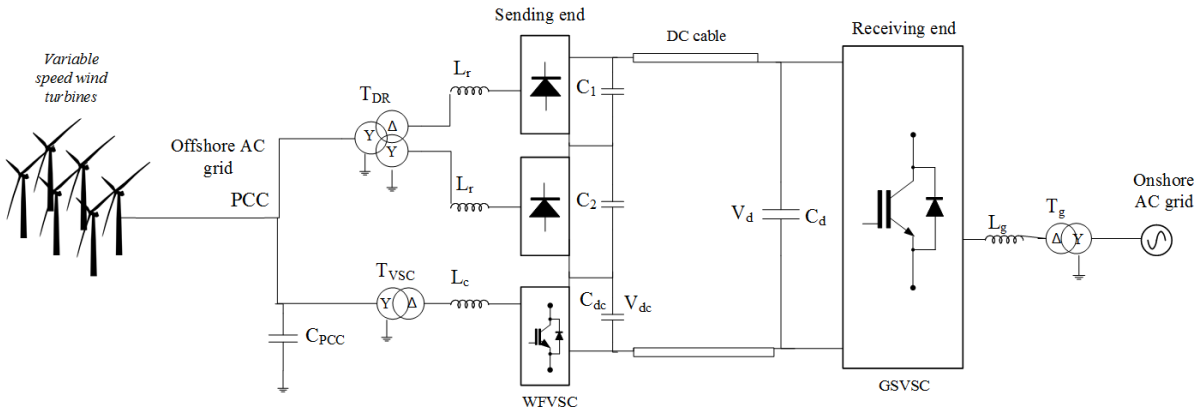

Figure 2.4: Hybrid HVDC-system utilizing a DR and a VSC connected in series [adapted from 12].

The hybrid topology has reduced switching losses compared to a VSC-based converter station of the same total power rating. This is because the power rating of the VSC is reduced, thus fewer switching devices are needed. The losses will still be greater than for the DR HVDC solution, but the converter footprint will be reduced a lot. Actually, according to Nguyen et al. [12] will the platform size be approximately the same as the VSC-based converter station because no passive filters are needed. The cost of the platform will be reduced compared to the VSC-HVDC because there are fewer expensive transistors and more robust DRs. The cost of power semiconductors and drivers for a 500 MW hybrid converter station was estimated to be 53.47% of a VSC-HVDC station in [12]. This estimate shows a significant reduction in price, which is why it is interesting to investigate this topology further.

2.5 Important Components

2.5.1 VSC

The detailed model of a VSC includes switching valves, where each valve consists of several insulated gate bipolar transistors (IGBTs) connected in series to achieve the required voltage level. The switches in this study are considered ideal without any time-delay or losses. The converter is able to operate in bidirectional power flow by connecting free-wheeling diodes in anti-parallel. A more detailed description of the switching devices can be studied in [20].

The advantage of using transistors in the switching valves is the fact that they can be turned on and off which makes them self-commutating. Due to this fact they become less dependent on a strong ac grid, unlike LCC, thus they can be switched at high frequency, i.e. in the range of kHz [7]. When the converter has a high switching frequency, it is able to eliminate the low order harmonics and control the phase shift between the output voltage and current on the ac side. This controllability means that the converter has full control over the active and reactive power and there is no need for bulky capacitors for reactive power compensation. The result is a compact converter which can be installed in places with limited space, e.g. offshore converter platforms. The VSC can also be used as an active filter to eliminate harmonic components in the ac voltage and this will be explained further in this thesis.

A six pulse, two level VSC configuration is shown in Fig. 2.5. The converter is connected to a three-phase voltage source on the ac side, through a resistance, R and a coupling inductance, L which represents the transformer and a phase reactor. The figure shows the grid voltages v_a, v_b and v_c, and grid currents i_a, i_b and i_c. Also, the voltages on the converter ac side is represented as V_{c1}, V_{c2}, and V_{c3}, and on the dc side the voltage is represented as $V_{dc} = \frac{v_{dc}}{2} + \frac{v_{dc}}{2}$.

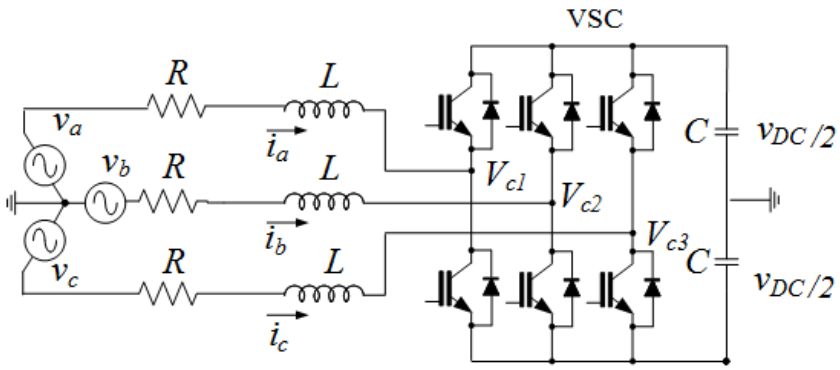

Figure 2.5: A detailed model of a VSC.

2.5.2 Harmonic Cancellation Transformer

Harmonics are introduced to the system by the DR and must be filtered out to avoid disturbance in the ac grid. If two six-pulse DRs (6P-DRs) are connected in series and connected with a three-winding transformer having a Y/Y/Δ-connection, as seen in Fig. 2.4, then the 5th- and 7th-order harmonic components of the phase currents are eliminated. This is because the connection gives a 30-degree shift in the phase voltages from each of the two bridge rectifiers, and the sum of them gives a twelve pulse instead of a six-pulse [21]. This results in a constant dc voltage and fewer harmonics in the offshore grid.

2.5.3 AC Filter

When a dc link connects separate power systems, either with synchronous frequency or not, there will be a wide spectrum of harmonic and non-harmonic frequency transfers [22]. These harmonics will cause distortion of the voltages and the currents, which will result in power losses and overheating in electrical equipment. To reduce the effect of the harmonic distortion, either an APF or an ac filter should be applied. The ac filter is connected in shunt with the harmonic load and will filter out specific low-order harmonics by introducing a low impedance. Passive filter tuning of a shunt filter is described in Appendix A and more details on the ac filters can be found in [23], [24] and [25].

2.5.4 Passive Elements

Passive elements are used as filters and as energy storage. Energy stored in the ac side of the VSC is less than 5% of all energy stored, thus most of the energy is stored in the dc capacitor which ensures a stable dc voltage. During the fast switching pulse width modulation (PWM), explained in Section 3.3, the passive elements are charged and discharged to ensure smooth ac currents and dc voltage. The filters affect the control abilities, and overall design is a compromise between high filtering and fast dynamic performance [26].

Phase Reactor

A phase reactor connected in series with the harmonic load will prevent high-order harmonics from entering the system. The series filter will help to stabilize the ac current by reducing harmonic content produced by the converter, as well as reducing the fault current. The transformer will also provide some phase inductance, but the larger share is provided by the phase reactor. The reactance of the phase reactor must be 10-15% of the base impedance to eliminate the high order harmonics. The phase reactor is calculated as follows:

$$L = \frac{X_L}{\omega} \quad \text{where } X_L = 0.15 Z_b \quad \text{and } Z_b = \frac{V_s^2}{P}.$$

V_s is the rated line to line RMS voltage and P is the rated active power absorbed by the converter at rated grid frequency ω.

2.5.5 Capacitor

- DC capacitors help to maintain a stable and smooth dc voltage by reducing voltage ripples and harmonics produced by the converter valves [11]. They will also provide the energy needed to stabilize the real power difference in transient events. The value is calculated as follows [27]:

$$C \geq \frac{T_r \Delta P_{MAX}}{2 V_d \Delta V_d}$$

where

1. T_r is the time delay constant, introduced by the filtering of dc voltage and current control.
2. ΔV_d is the tolerable dc voltage variation.
3. ΔP_{MAX} is the maximum known power variation on the dc bus.

It can be seen that a fast dc voltage loop, i.e. small time constant, will be in contrast to a small variation in dc voltage and a large allowable power variation. A fast voltage loop can be accomplished by using a small capacitor, but the other two aims will need a larger capacitor. Also the cost and available space will limit the size of C.

- A single capacitor is utilized to stabilize the ac voltage by filtering the switching frequency harmonics that can interfere with other equipment. The capacitor value is calculated from the definition of the resonant frequency:

$$\omega_{res} = \frac{\omega_s}{10} = \frac{1}{\sqrt{LC}}$$

where L is the value of the phase reactor and ω_s is the switching frequency.

2.6 Summary

This chapter introduced important issues regarding integration of OWFs. OWFs will affect system stability in power grids with high penetration of wind energy and the converter interfaces used for integration will produce harmonic content which will distort the voltage. It is important to know about these issues concerning OWF integration, which is why they were presented in this chapter.

The three system topologies utilized to integrate OWFs were presented and some of the advantages and disadvantages of each solution were commented. The size of the converter platform and the number of switching devices are important factors that decide if one solution is better than another. Also, the ability to control the converter is an important factor which will be presented in the next chapter. In the end, some important components of the system were explained more in detail to get a better understanding of the topologies.

Chapter 3

Control of Offshore Converter

3.1 Introduction

The controllability of the offshore converter in the HVDC link provides more flexibility to the system. If the converter is able to control the ac voltage, then the WF can control the power point tracking, such that maximum power can be extracted from the wind. If the converter can be controlled to provide harmonic cancellation and reactive power compensation, then fewer bulky capacitors and filters are needed and the converter platform size can be reduced.

It is important to define the control objectives in order to design the controller. The control objectives define which of the parameters that must be controlled, and how complex the controller will be. The three converter solutions presented in this thesis have different control objectives, which will be presented in this chapter. Moreover, important concepts relevant to the controller will be explained before the controllers are designed in the next chapters.

3.2 Control Objectives

3.2.1 Diode-Based HVDC link

There are no control objectives for the offshore converter platform in the diode-based HVDC link solution because the diode rectifiers are uncontrollable. The topology must take advantage of the modern wind farm technology by utilizing an FRC-WT which decouples the WT from the offshore ac grid. The advantage of the FRC-WT is that its control objectives can be altered such that the ac grid can be controlled. The control solution by Blasco et al. [9] proposes that the front-end inverter will control the offshore ac voltage instead of the dc voltage, and thus the back-end inverter must control the dc voltage. Because the control objective of the back-end inverter is altered, the WF is no longer able to control the active power point tracker. This is a disadvantage because the maximum power extraction is not obtained and available power is lost.

3.2.2 APF-DR Topology

There are two control objectives for the APF solution because the APF is connected in shunt and is therefore based on the harmonic current cancellation concept. The objectives are:

1. The APF will inject a current $\boldsymbol{i_{APF}}$ which must eliminate the harmonic content from the load current $\boldsymbol{i_L}$, i.e. force the source current $\boldsymbol{i_s}$ to track a reference $\boldsymbol{i_s^*}$ [1] which is proportional to the source voltage V_s. This control objective is called *harmonic control*.

$$\boldsymbol{i_s} \rightarrow \boldsymbol{i_s^*} = g\boldsymbol{V_s}$$

2. The APF must control the dc voltage V_{dc} to a constant and predefined value such that maximum energy in the capacitor is always available, and thus the APF can contribute with harmonic cancellation and reactive power compensation.

$$V_{dc} \rightarrow V_{dc}^*$$

[1] The notation $(.)^*$ stands for reference value and will be used throughout this thesis.

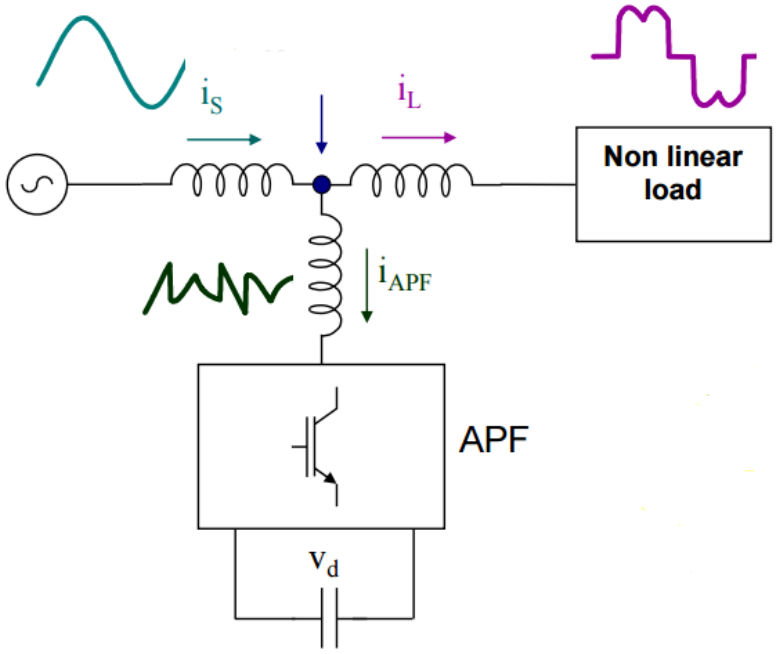

Figure 3.1: Principle of the shunt connected APF operation [28].

It can be seen in Fig. 3.1 that the source current $\boldsymbol{i_s} = \boldsymbol{i_L} + \boldsymbol{i_{APF}}$, where the converter current has the opposite sign of the harmonic current component of the load current: $\boldsymbol{i_{APF}} = -\boldsymbol{i_{Lh}}$. The opposite sign makes the APF inject a current that will compensate for the harmonic distortion. As a consequence, the source current will be purely sinusoidal and the control objective is fulfilled.

3.2.3 Hybrid DR-VSC Topology

There are three control objectives for the WFVSC:

1. *Voltage tracking control* is applied to regulate the grid voltage to a specified voltage magnitude and frequency, $\boldsymbol{V_s} \rightarrow \boldsymbol{V_s^*}(m, f)$. The voltage error must go toward zero $\tilde{\boldsymbol{V}}_{\boldsymbol{s}} \rightarrow 0$ when $t \rightarrow \infty$ to obtain perfect tracking $\boldsymbol{V_s} = \boldsymbol{V_s^*}$.

2. *Harmonic control* is applied to make the VSC work as an APF by injecting a current which contains all the harmonics represented in the system.

3. *Balancing control* is applied to force the dc voltage of the VSC to a constant and predefined value $V_{dc} \rightarrow V_{dc}^*$. The total dc-link voltage V_d will then be balanced between the 12P-DR and the VSC. The magnitude of the dc voltage V_{dc}^* must be large

enough such that the VSC can compensate for reactive power and harmonic components. Also, it is desirable to keep the rating of the VSC small, such that fewer switching devices are needed and thus the total cost of the converter can be reduced.

The control objectives of the GSVSC are the same as for the conventional VSC-HVDC transmission system. The control objectives are dc-link voltage control, i.e. securing fully power transmission to the onshore grid, and control of reactive power delivered to the ac grid. Only the control of the WFVSC will be studied because the control of the GSVSC is not in the scope of this thesis.

3.3 Pulse Width Modulation

PWM is a controlling technique that results in high-frequency switching valves [18]. A carrier signal consisting of a triangular waveform, with high frequency (kHz), is compared to a modulating signal in a PWM generator. The PWM generator produces a control signal which is sent to the switches and tells them which position they should stay in. The modulation ratio m_a is defined as the magnitude of the modulating signal divided by the magnitude of the carrier signal: $m_a = \frac{|V_c|}{|V_{tri}|}$. It is important to avoid over-modulation, $m_a > 1.0$, because then the converter will produce more harmonics. The modulating ratio chosen will affect the output ac voltage defined in [18] and shown in (3.1). When the voltage over one of the inverter legs is equal to $\frac{V_{dc}}{2}$, the output ac voltage is defined as:

$$V_{LL} = \sqrt{\frac{3}{2}} m_a \frac{V_{dc}}{2} \tag{3.1}$$

3.4 Stationary Reference Frame

One of the objectives of this thesis is to design a control scheme in the stationary reference frame, i.e $\alpha\beta$-frame. A benefit from using the $\alpha\beta$-frame is that the system is transformed from a three-phased system to a two-phased, which makes the control design easier. Another advantage is that there is no need for a phase locked loop (PLL) which calculates the phase angle of the system. This angle is used to calculate the rotating reference frame which is applied to the hybrid topology in [12]. A simple PLL is sensitive to harmonics in the input voltage and can calculate the wrong phase angle which will affect the controller and the control signal sent to the switching valves [29]. The fact that active and reactive power can be decoupled in the rotating reference frame is not possible in the $\alpha\beta$-frame [30]. The disadvantage of not being able to decouple the active and reactive power is that the controller is more complex. The method utilizing the rotating reference frame will not be discussed further in this thesis, but a thesis by Bajracharya [31] gives a detailed explanation of this control method.

Clarke transformation is applied to the three-phased system to convert it into $\alpha\beta$-frame, and the transformation is shown in Appendix B.

3.5 Control of Unbalanced and Distorted Signals

When designing a control system it is important to think of a scenario where a fault occurs, which results in an unbalanced system. It is also important to think of the harmonics introduced by power electronic devices, which will distort the voltage or current. The controller must be able to regulate such a system, and thus the equation for this system must be considered in the control design.

The load current $i_{d_{\alpha\beta}}$ and source voltage $V_{s_{\alpha\beta}}$ are assumed to be distorted and unbalanced periodic signals such that the model-based control design in this thesis can be applied to any system. The signals contain higher order harmonics of the fundamental frequency ω

and becomes

$$i_{d_{\alpha\beta}} = \sum_{k\in\chi} (\boldsymbol{e}^{\boldsymbol{J}k\omega t}\boldsymbol{I}^{p}_{d,k} + \boldsymbol{e}^{-\boldsymbol{J}k\omega t}\boldsymbol{I}^{n}_{d,k})$$
$$V_{s_{\alpha\beta}} = \sum_{k\in\chi} (\boldsymbol{e}^{\boldsymbol{J}k\omega t}\boldsymbol{V}^{p}_{s,k} + \boldsymbol{e}^{-\boldsymbol{J}k\omega t}\boldsymbol{V}^{n}_{s,k})$$

where $\boldsymbol{e}^{\boldsymbol{J}k\omega t}$ is a rotation matrix of the form

$$\boldsymbol{e}^{\boldsymbol{J}k\omega t} = \begin{bmatrix} cos(\omega kt) & -sin(\omega kt) \\ sin(\omega kt) & cos(\omega kt) \end{bmatrix}$$
$$\boldsymbol{e}^{\boldsymbol{J}k\omega t} = (\boldsymbol{e}^{\boldsymbol{J}k\omega t})^{T}, \quad \boldsymbol{J} = \begin{bmatrix} 0 & -1 \\ 1 & 0 \end{bmatrix}.$$

Vectors $\boldsymbol{I}^{p}_{d,k}, \boldsymbol{I}^{n}_{d,k} \in \mathbb{R}^2$ are the k^{th} harmonic coefficients for the positive- and negative-sequence representation of the load current. $\boldsymbol{V}^{p}_{s,k}, \boldsymbol{V}^{n}_{s,k} \in \mathbb{R}^2$ are the same representations for the source voltage and $\chi = \{1,2,3,...\}$ is the set of selected harmonics indices. The time derivatives are derived as follows:

$$\frac{di_{d_{\alpha\beta}}}{dt} = \boldsymbol{J}\omega \sum_{k\in\chi} k(\boldsymbol{e}^{\boldsymbol{J}k\omega t}\boldsymbol{I}^{p}_{d,k} - \boldsymbol{e}^{-\boldsymbol{J}k\omega t}\boldsymbol{I}^{n}_{d,k})$$
$$\frac{dV_{s_{\alpha\beta}}}{dt} = \boldsymbol{J}\omega \sum_{k\in\chi} k(\boldsymbol{e}^{\boldsymbol{J}k\omega t}\boldsymbol{V}^{p}_{s,k} - \boldsymbol{e}^{-\boldsymbol{J}k\omega t}\boldsymbol{V}^{n}_{s,k}) \tag{3.2}$$

The derivatives are signals which can not be computed in a straightforward manner, and will be lumped together in a parameter which is estimated in the control design. The Lyapunov approach is used to find an estimate for the lumped parameter, and this theory is introduced in the next section.

3.6 Passivity-Based Control Theory

The passivity-based control (PBC) theory will be explained briefly to give the reader a better understanding of the control design in Section 5.4. The PBC theory presented in [32] may be viewed as an extension to the well-known energy-shaping plus damping injection (ESDI) technique. There are two basic stages for this technique [32];

1. *Damping injection* stage: The controller is modified to ensure asymptotic stability by adding damping terms which are proportional to the system errors.
2. *Energy shaping* stage: A Lyapunov function is chosen, which has some characteristics [33]:
   (a) It is a continuous differential function.
   (b) It has to be positive semidefinite; which means that the function is bigger or equal to zero.
   (c) Its derivative along the trajectories has to be negative semidefinite; which means that the function is less or equal to zero.

   The Lyapunov function can also be called the energy function, which is why the stage is called energy shaping. If the energy equation fulfills the characteristics, then the system will be stable and converge towards a minimum when it is in equilibrium. LaSalle's theorem can be applied to prove the asymptotic stability, and this theory can be studied in [32]. The theory is outside the scope of this thesis, thus no further details will be given.

The Lyapunov approach is used to make conclusions about the trajectories of a system without finding them, i.e. solving the differential equation [34]. The approach is used to estimate the unknown parameters which are influenced by the harmonic content introduced by the distorting load. These parameters can not be calculated in a straightforward manner, thus they are lumped together in a parameter which is estimated by proposing adaptive laws. The Lyapunov stability theorem in [32] is used to find the adaptive laws which will make sure that the equilibrium point is stable by having a unique minimum of the potential energy function. The procedure is as follows:

1. A Lyapunov function for the system, which fulfills the characteristics, is proposed.

2. The derivative of the function is calculated along the trajectories.
3. Adaptive laws are proposed, which forces the derivative along the trajectories to be negative semidefinite.
4. The adaptive laws are transformed in a way such that they can represent the lumped parameter in the block diagram of the system controller.

The controllers that are designed in this thesis follow the procedure mentioned above.

3.7 Summary

The three converter topologies presented in this thesis have different control objectives. It was important to know the control objectives before the controller was designed, such that one can know which parameters to control. The passivity-based control design procedure was explained and a step by step procedure was proposed which is applied for the control design in this thesis. PWM and control design in stationary reference frame was briefly explained to give the reader a basic understanding of the control design applied in this thesis.

Chapter 4

Active Power Filter

4.1 Introduction

The harmonics and reactive power in the diode-based HVDC link in [9] are compensated by passive filters and capacitors respectively. A disadvantage of the topology is that the filter banks and capacitors have a large footprint and space on an offshore platform is limited. Another disadvantage is the fact that they can be mistuned and have resonance with the load or impedance [11]. Because of these drawbacks, the active power filters (APFs) have become an alternative solution for reactive power and harmonic compensation.

The APFs have certain advantages which the passive filters do not have. The APFs are flexible and adaptable because they are controllable, and the topology is compact and requires a smaller space than passive filters. Another advantage is the controllability of the power devices used in the APFs, which makes them able to provide both harmonic and reactive power compensation [35]. A drawback of the APFs is the fact that they are expensive because of the fast-switching power electronic devices. It will become more expensive with higher power capacity because more switching devices are needed to carry the current and withstand the voltage.

APFs are not normal in high-voltage grids because they are expensive and the THD tends to be smaller than in medium-voltage grids of 6.6 kV [36]. The reason is that high-voltage systems are stiffer and thus there will be fewer harmonics to compensate. But there are some high-voltage/power systems where harmonics are introduced by converters based on

thyristors or diodes. In Japan, several shunt active filters in a range of 40 MVA to 60 MVA have been installed in substations along the Tokaido Shinkansen to eliminate harmonics introduced by thyristor controlled rectifiers [11]. Another area where APFs can be beneficial in the future is in offshore grids where the converter station needs to be small and both reactive power and harmonics must be compensated.

The purpose of this chapter is to show how the passivity-based control (PBC) theory, introduced in Section 3.6, can be used to design a controller for the APF-DR topology.The PBC procedure from Ch. 3.6 will be developed step by step for the APF in order to design the controller for the hybrid DR-VSC topology.

4.2 Model Topology

The topology for the simulation model utilized in this study for the APF control is shown in Fig. 4.1. The harmonic content producing 12P-DR load is connected to an ideal voltage source representing the wind farm. A shunt connected APF is connected to the system for harmonic and reactive power compensation, instead of passive filters and compensating capacitors as in [9]. A resistance R_L is connected to the dc side of the DR to represent the load[1], and a resistance R is connected to the dc side of the VSC. The resistance R has a high value and thus the losses can be neglected because they are quite small. The load R is represented in Fig. 4.1 for control design purposes, but it is neglected in the simulations because of the low losses.

A three-winding transformer is connected to the two 6P-DRs in a $Y/Y/\Delta$-configuration to give a 12P-DR as explained in Section 4.3. A load R_T is added to one of the star connections to isolate it from the ground such that it will be equal to the Δ-connection, which is naturally isolated from ground. The leakage reactance of the transformer X_T and all the system parameters are given in Table 4.1. The dc capacitor C_{dc} must be sufficiently large enough because it is used to provide reactive power and harmonic support. Also, the dc voltage must be kept constant by the controller such that maximum energy is always available.

[1]The power flow from the WF has the same direction and the same harmonic content as the model utilizing an ideal voltage source connected to a 12P-DR, where the load is a resistance.

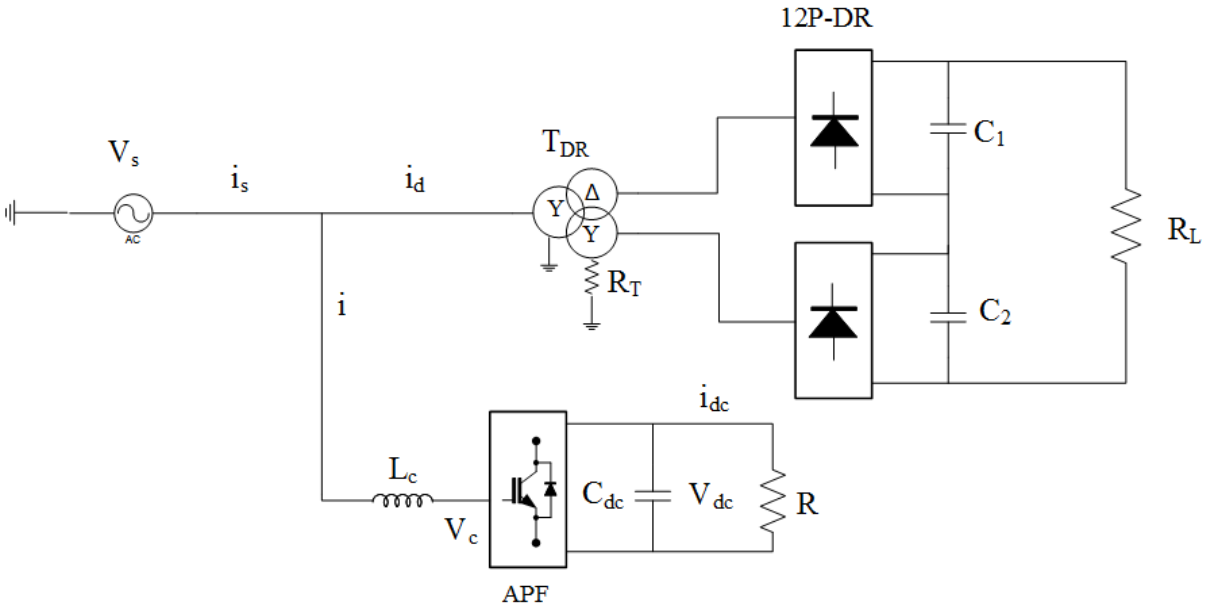

Figure 4.1: The simulation model for the study of APF control.

Table 4.1: System Parameters for APF

Power and Voltage	**Parameters**	**Values**	Unit
Base values	Power rating	400	MVA
	AC Voltage	33	kV
	frequency	50	Hz
Passive elements	C_1	300	μF
	C_2	300	μF
	C_{dc}	300	μF
	L_c	13	mH
	R_L	100	Ω
	R_T	1	MΩ
Transformer	T_{DR}	33/76/76	kV
	X_T	0.1	p.u.

4.3 Control Design

4.3.1 System Equations

This section shows the development of the control design for the APF and [37] is taken as a reference. The system equations are obtained from Fig. 4.1, where equation (5.1) is derived by applying Kirchhoff's Voltage Law (KVL) and (4.2) is derived from the power balance over the lossless VSC:

$$L_c \frac{d\boldsymbol{i}(\boldsymbol{t})}{dt} = \boldsymbol{V_s}(\boldsymbol{t}) - \frac{V_{dc}(t)}{2}\boldsymbol{\delta}(\boldsymbol{t}) \tag{4.1}$$

$$C_{dc}\frac{dV_{dc}(t)}{dt} = \frac{\boldsymbol{\delta}(\boldsymbol{t})^T \boldsymbol{i}(\boldsymbol{t})}{2} - \frac{V_{dc}(t)}{R} \tag{4.2}$$

where the inductor resistance is neglected because it only adds damping to the system. The grid voltage, $\boldsymbol{V_s}(\boldsymbol{t})$ and converter current, $\boldsymbol{i}(\boldsymbol{t})$. They are given as balanced three-phase vectors $\boldsymbol{X}(\boldsymbol{t}) = [X_a(t) \quad X_b(t) \quad X_c(t)]^T$.

$$\begin{aligned} X_a(t) &= \hat{X}\cos\theta(t) \\ X_b(t) &= \hat{X}\cos\left(\theta(t) - \frac{2}{3}\pi\right) \\ X_c(t) &= \hat{X}\cos\left(\theta(t) + \frac{2}{3}\pi\right) \end{aligned}$$

where $\hat{X}$ represents the peak value of the parameter X. $\boldsymbol{\delta}(\boldsymbol{t})$ is the switch positions for each converter leg: $\begin{bmatrix}\delta_1 & \delta_2 & \delta_3\end{bmatrix}^T \in \{-1,1\}^3$. The discrete system will be transformed into a continuous system by assuming that an average model is possible because the switching frequency is sufficiently high enough when PWM technique is applied [37].

For control purposes it is useful to express the control currents $\boldsymbol{i}(\boldsymbol{t})$ in terms of the source currents $\boldsymbol{i_s}(\boldsymbol{t})$ in (4.1)

$$\boldsymbol{i}(\boldsymbol{t}) = \boldsymbol{i_s}(\boldsymbol{t}) - \boldsymbol{i_d}(\boldsymbol{t}) \tag{4.3}$$

4.3.2 Average Model in Stationary Reference Frame

The average model will be developed for control design purposes, based on the assumption that the switching vector $\boldsymbol{\delta(t)}$ in (4.2) can be replaced by the duty ratio $\boldsymbol{u(t)} = [u_a \quad u_b \quad u_c]^T, \in [-1, 1]$, which is an approximation of the actual controller and a continuous signal. With these considerations, and by inserting (4.3) in the system equation, the *average model* is obtained:

$$\begin{aligned} L_c \frac{d\boldsymbol{i_s(t)}}{dt} &= \boldsymbol{V_s(t)} - \boldsymbol{\varphi(t)} + L_c \frac{d\boldsymbol{i_d(t)}}{dt} \\ C_{dc} \frac{dV_{dc}(t)}{dt} &= \frac{\boldsymbol{u(t)}^T(\boldsymbol{i(t)} - \boldsymbol{i_d(t)})}{2} - \frac{V_{dc}(t)}{R}. \end{aligned} \tag{4.4}$$

where the control input $\boldsymbol{\varphi(t)} = \frac{V_{dc}(t)}{2}\boldsymbol{u(t)}$.

By applying Clarke transformation[2]to the average model (4.4), the model can be described in a two-phased stationary reference frame as:

$$L_c \frac{di_{s_{\alpha\beta}}}{dt} = V_{s_{\alpha\beta}} - \varphi_{\alpha\beta} + L_c \frac{di_{d_{\alpha\beta}}}{dt} \tag{4.5}$$

$$C_{dc} \frac{d}{dt}\left(\frac{V_{dc}^2}{2}\right) = \varphi_{\alpha\beta}^T (i_{s_{\alpha\beta}} - i_{d_{\alpha\beta}}) - \frac{V_{dc}^2}{R} \tag{4.6}$$

where the new control signal is defined as $\varphi_{\alpha\beta} \triangleq V_{dc} u_{\alpha\beta}/2$ [37] and where the parameters are defined as follows, $i_{s_{\alpha\beta}} = [i_{s_\alpha} i_{s_\beta}]^T, i_{d_{\alpha\beta}} = [i_{d_\alpha} i_{d_\beta}]^T, V_{s_{\alpha\beta}} = [V_{s_\alpha} V_{s_\beta}]^T$.

In the next steps of control design, it is assumed that the current dynamics of (4.5) has a much faster response than the capacitor dynamics of (4.6) [37]. By applying this assumption, the complexity of the control design is reduced by splitting it into two stages: inner loop (current control design) and outer loop (voltage control design) where the outer loop is designed to give optimum regulation and stability [38].

[2]See Appendix B for transformation.

4.3.3 Inner Control Loop

An adaptive controller, based on passivity control theory [32] is utilized for a STATCOM in [37], and the same control system is applied for the APF in this study. The design of the inner control loop is based on the ESDI technique explained in Section 3.6. The ESDI technique has two parts:

1. The damping injection stage is applied to subsystem (4.5), where the desired reference $i^*_{s_{\alpha\beta}}$ replace the state $i_{s_{\alpha\beta}}$ and a damping term is added:

$$L_c \frac{d i^*_{s_{\alpha\beta}}}{dt} = V_{s_{\alpha\beta}} - \varphi_{\alpha\beta} + L_c \frac{d i_{d_{\alpha\beta}}}{dt} + \boldsymbol{K_1} \tilde{i}_{s_{\alpha\beta}} \tag{4.7}$$

   where $\tilde{i}_{s_{\alpha\beta}} \triangleq i_{s_{\alpha\beta}} - i^*_{s_{\alpha\beta}}$ and $\boldsymbol{K_1}$ is a positive-definite design matrix which is used to introduce damping in the system.

2. The derivative terms in (4.7) can not be computed in a straightforward manner because both currents (i_s, i_d) are distorted by the DR. The controller proposed in [37] includes a parameter that lumps all harmonic coefficients together in one *lumped parameter*, $\hat{\phi}_{k_{\alpha\beta}}$[3]. The resulting controller is expressed as

$$\varphi_{\alpha\beta} = \sum_{k\in\chi} \hat{\phi}_{k_{\alpha\beta}} + V_{s_{\alpha\beta}} + \boldsymbol{K_1} \tilde{i}_{s_{\alpha\beta}}. \tag{4.8}$$

The lumped parameter $\hat{\phi}_{k_{\alpha\beta}}$ is estimated by following the Lyapunov approach 3.6. This approach is explained more in detail in the next chapter, but the main parts are mentioned here:

1. To begin with, a Lyapunov function is proposed which must be a positive-definite function that is forced to decrease along the trajectories of the system [37].

$$W = \frac{L}{2} \tilde{i}^T_{s_{\alpha\beta}} \tilde{i}_{s_{\alpha\beta}} + \sum_{k\in\chi} \frac{1}{2\gamma_k} \left[(\tilde{\Phi}^p_k)^2 + (\tilde{\Phi}^n_k)^2 \right]$$

[3]The notation $\hat{(.)}$ denotes the estimated value throughout this report.

2. Then the derivative of the Lyapunov function is calculated along the trajectories of the system.

$$\dot{W} = -\boldsymbol{K_1}\tilde{i}_{s_{\alpha\beta}}^{T}\tilde{i}_{s_{\alpha\beta}} - \tilde{i}_{s_{\alpha\beta}}^{T}\sum_{k\in\chi}\left(e^{\boldsymbol{J}k\omega t}\tilde{\Phi}_k^p + e^{-\boldsymbol{J}k\omega t}\tilde{\Phi}_k^n\right) + \sum_{k\in\chi}\frac{1}{\gamma_k}\left[(\dot{\tilde{\Phi}}_k^p)^T\tilde{\Phi}_k^p + (\dot{\tilde{\Phi}}_k^n)^T\tilde{\Phi}_k^n\right]$$

3. Adaptive laws which are forcing the derivative of the Lyapunov function to be negative semidefinite are proposed. The adaptive laws proposed by Escobar et al. for the STATCOM in [37] are:

$$\dot{\hat{\phi}}_k^p = \gamma_k\tilde{i}_{s_{\alpha\beta}} - \boldsymbol{J}k\omega\hat{\phi}_k^p, \quad k\in\mathbb{R}$$
$$\dot{\hat{\phi}}_k^n = \gamma_k\tilde{i}_{s_{\alpha\beta}} - \boldsymbol{J}k\omega\hat{\phi}_k^n, \quad k\in\mathbb{R}$$
$$\boldsymbol{J} = \begin{bmatrix} 0 & -1 \\ 1 & 0 \end{bmatrix}$$

where γ_k is a design parameter used to eliminate the specific harmonic component k. Both the positive- and the negative-sequence components are taken into consideration, such that the controller can be applied to unbalanced systems.

4. Laplace transformation is applied to the adaptive laws such that they can be applied in the block diagram of the controller. The resulting transfer function in positive- and negative sequence is:

$$\hat{\phi}_k^p = \frac{\gamma_k\tilde{i}_{s_{\alpha\beta}}}{s+\boldsymbol{J}k\omega}$$
$$\hat{\phi}_k^n = \frac{\gamma_k\tilde{i}_{s_{\alpha\beta}}}{s-\boldsymbol{J}k\omega}.$$

Then finally the lumped parameter is defined as

$$\begin{aligned}
&\hat{\phi}_{k_{\alpha\beta}} \triangleq \hat{\phi}_k^p + \hat{\phi}_k^n \in \mathbb{R}^2 \\
&= \gamma_k \tilde{i}_{s_{\alpha\beta}} \Big[\frac{1}{s + \boldsymbol{J}k\omega} + \frac{1}{s - \boldsymbol{J}k\omega} \Big] \\
&= \gamma_k \tilde{i}_{s_{\alpha\beta}} \Big[\frac{s - \boldsymbol{J}k\omega}{(s + \boldsymbol{J}k\omega)(s - \boldsymbol{J}k\omega)} + \frac{s + \boldsymbol{J}k\omega}{(s + \boldsymbol{J}k\omega)(s - \boldsymbol{J}k\omega)} \Big] \\
&= \gamma_k \tilde{i}_{s_{\alpha\beta}} \Big[\frac{s + s}{s^2 - (\boldsymbol{J}k\omega)^2} \Big], \quad \boldsymbol{J}^2 = \begin{bmatrix} -1 & 0 \\ 0 & -1 \end{bmatrix} \\
&= \frac{2\gamma_k s}{s^2 + k^2\omega^2} \tilde{i}_{s_{\alpha\beta}}
\end{aligned}$$

where s is the Laplace complex variable. The resulting controller includes a resonant filter tuned to the frequency for the selected harmonics [39]. The resonant filter has an infinite gain at the resonant frequency which makes it difficult to tune the filters in the simulation. Bandpass filters (BPFs) have been used to guarantee safer operation. A damping term in the denominator of the BPF transfer function limits the gain, which makes it easier to tune the filters in the simulation. Thus the final lumped parameter becomes:

$$\hat{\phi}_{k_{\alpha\beta}} = \frac{2\gamma_k s}{s^2 + sk\omega/Q_k + k^2\omega^2} \tilde{i}_{s_{\alpha\beta}} \tag{4.9}$$

where Q_k is the quality factor.

4.3.4 Outer Control Loop

The control objective for the outer loop is to drive the dc voltage to a predefined constant reference V_{dc}^*. The outer loop must add damping to the system such that the asymptotic stability of the closed loop is reinforced and it should incorporate robustness to uncertainties in the control parameters [37]. It is assumed that the dynamics of the inner loop is much faster that the outer loop, thus after short time the source current is able to track the reference current perfectly and it can be further assumed that $i_{s_{\alpha\beta}} \approx i_{s_{\alpha\beta}}^* = gV_{s_{\alpha\beta}}$, $\tilde{i}_{s_{\alpha\beta}} = 0$ and $\hat{\phi}_{k_{\alpha\beta}} = \phi_{k_{\alpha\beta}}$. Controller (4.8) is substituted in (4.6) and yields the following expression:

$$C_{dc}\frac{dz}{dt} = (gV_{s_{\alpha\beta}}^T - i_{d_{\alpha\beta}}^T)(\sum_{k\in\chi}\hat{\phi}_{k_{\alpha\beta}} + V_{s_{\alpha\beta}}) - \frac{2z}{R}$$
$$= g(V_{s_{\alpha\beta}}^T V_{s_{\alpha\beta}} + V_{s_{\alpha\beta}}^T \sum_{k\in\chi}\hat{\phi}_{k_{\alpha\beta}}) - (i_{d_{\alpha\beta}}^T \sum_{k\in\chi}\hat{\phi}_{k_{\alpha\beta}} + i_{d_{\alpha\beta}}^T V_{s_{\alpha\beta}}) - \frac{2z}{R}$$

where $z \triangleq V_{dc}^2/2$ for simplicity. The error dynamics of this system are

$$\begin{aligned} C_{dc}\frac{d\tilde{z}}{dt} &= gc_1 - c_2 - \frac{2\tilde{z}}{R} \\ c_1 &= V_{s_{\alpha\beta}}^T V_{s_{\alpha\beta}} + V_{s_{\alpha\beta}}^T \sum_{k\in\chi}\hat{\phi}_{k_{\alpha\beta}} \\ c_2 &= i_{d_{\alpha\beta}}^T \sum_{k\in\chi}\hat{\phi}_{k_{\alpha\beta}} + i_{d_{\alpha\beta}}^T V_{s_{\alpha\beta}} \end{aligned} \tag{4.10}$$

where $\tilde{z} \triangleq z - z^*, \quad z^* = \frac{V_{dc}^*}{2}$. Parameters c_1 and c_2 are assumed to be unknown and $V_{s_{\alpha\beta}}^T V_{s_{\alpha\beta}} = V_{s,RMS}^2$. Remark: $|V_{s_{\alpha\beta}}^T \sum_{k\in\chi}\hat{\phi}_{k_{\alpha\beta}}| \ll V_{s,RMS}^2$, thus $c_1 > 0$.

The error dynamic system (4.10) is a linear time-invariant (LTI) system where the state $\tilde{z}$ is the output and the g is the control input, which is disturbed by the constant signal c_2. For this stable system, a proportional plus integral controller (PI controller) can be utilized to fulfill the control objective [37]

$$g = -\left(\frac{k_i}{s} + k_p\right)\tilde{z} \tag{4.11}$$

where k_p is the proportional constant and $k_i = k_p/T_i$ is the integral constant where T_i is the integral time constant. The proportional gain g is the conductance observed by the power source which makes the source current follow the source voltage proportionally.

Notice that all control expressions are independent of system parameters, besides the frequency ω, which makes the controller robust to uncertainties in the system parameters. This controller will be able to absorb step changes and slow variations in the parameters, and it will remain valid for unbalanced conditions because the negative-sequence component is taken into consideration in the control derivation in [37]. The block diagram of the controller is shown in Fig. 4.2 and, as mentioned before, it is adapted from the

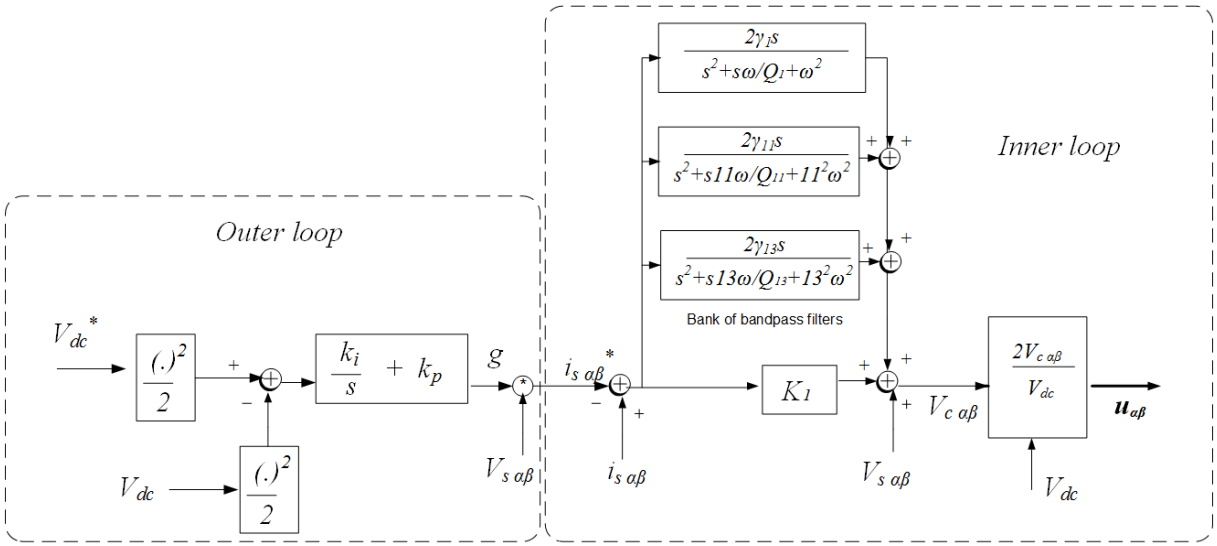

Figure 4.2: Block diagram of the controller utilized for the APF [adapted from][37].

controller proposed by Escobar et al. in [37].

4.4 Simulation Procedure

It is important to simulate in a step by step procedure to ensure that all components work properly. The procedure went as follows:

1. A 6P-DR was connected as a load to an ideal voltage source and the load current was measured.

2. The load was changed from a 6p-DR to a 12P-DR and the harmonic spectrum of the load current was measured to see which harmonics had to be compensated by the APF.

3. The APF was connected in shunt to the load, where the outer loop conductance value g was represented by a pre-calculated value. Also, no filter-blocks were included in the controller. The damping constant K_1 was tuned by the trial and error method.

4. Value g was replaced by the outer loop controller and the PI-control parameters were tuned.

5. The selected harmonic compensation blocks were included one at a time and tuned to eliminate the specific harmonic component of the load current.

4.5 Tuning of Control Parameters

The control parameters were found by the trial and error approach performed in a systematical way. The procedure went as follows:

1. First, the damping constant of the inner loop was tuned when $g = P/V_s^2 = 400/33^2 \approx 0.367$:
   (a) The error and the modulation function was measured.
   (b) The damping constant was increased incrementally, as long as the controller was not over-modulated until the error was at its minimum.
   (c) When the error did not change that much, the final value was chosen.
2. The outer loop was included where g was calculated by (4.11)
   (a) The error and the modulation function was measured.
   (b) The proportional gain was set to a low value because of the error measured and the time constant was set to a high value.
   (c) The gain was decreased until the change in the measured error was minimized and the time constant was increased until there was no change in the measured error. The outer controller was not fine-tuned.
3. The filters for the fundamental frequency, 11th- and 13th- harmonic component was included one by one and tuned in the same way by the trial and error method.
   (a) The THD and the modulation function was measured.
   (b) Parameter γ_k was increased until there was no change in the THD, and the modulating signal $\boldsymbol{u}$ was always kept lower than 1, to avoid over-modulation. If it was out of bound, the parameter was decreased until it was within limits.
   (c) Parameter Q_k was tuned in the same way, only this parameter had to be decreased because the THD did increase when the value was augmented. When there was no more change the previously measured parameter was kept.

It is important to emphasize that the tuning is not perfect and a more precise tuning procedure should be applied in future work. The parameters which were used in the

simulation are shown in Table 4.2.

Table 4.2: Control Parameters for APF

Inner Loop		K_1	20
Q_1	1	γ_1	70 000
Q_{11}	0.5	γ_{11}	400 000
Q_{13}	0.5	γ_{13}	400 000
Outer Loop			
k_p	0.00002	T_i	2000

4.6 Simulation Studies

4.6.1 Transformer Filtering

The effects of using a 12P-DR are the elimination of the 5th- and 7th- order harmonic current components. This is explained in Section 2.5.2 and Fig. 4.3 shows the load current in a 6P-DR and 12P-DR. It can be seen from the figure that the load current is much more distorted in the 6P-DR than in the 12P-DR. These results can be quantified by calculating the THD of the 6P-DR and the 12P-DR, which is 21% and 5% respectively. Thus the advantage of utilizing a 12P-DR is that the filters needed to eliminate the harmonics are reduced.

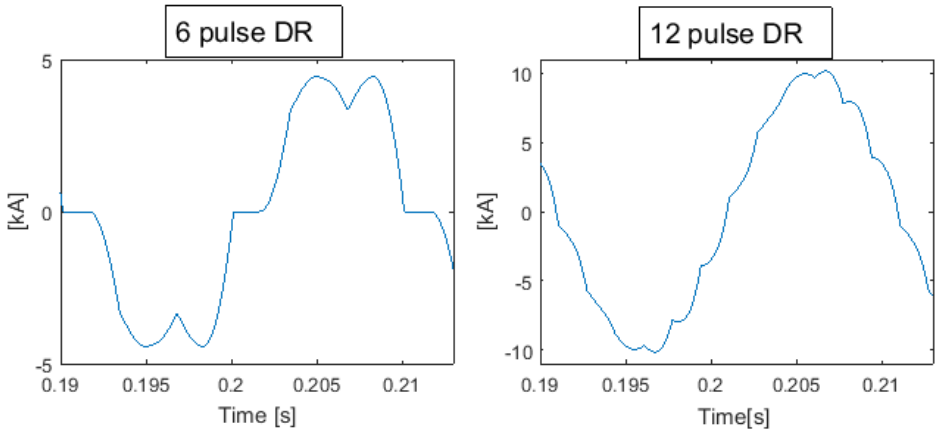

Figure 4.3: Current in a 6P-DR and a 12P-DR.

4.6.2 Reactive Power Compensation

There will be no reactive power or harmonic compensation before the APF is connected in shunt to the distorted load. It can be seen from Fig. 4.4 that the dashed line, which represents the reactive power when the APF is disconnected. The blue, whole line represents the reactive power when the APF is connected. The results show that there is a need for reactive power compensation when the APF is disconnected because $Q \neq 0$. The generating source, i.e. WF, must compensate for the reactive power in this scenario and thus a smaller amount of active power will be delivered to the load. Only active power delivered to the load results in economic income, which is why it is important that reactive effect is compensated by the APF.

In the upper graph in Fig. 4.5, it can be observed that the source voltage V_s and the source current i_s are out of phase. The power factor, $\cos\theta \neq 0$ when the APF is disconnected because there is reactive power in the system. The bottom graph represents V_s and i_s when the APF is connected, and it can be observed that they are in phase because $Q = 0$. This means that $\cos\theta = 0$ and all the active power will be equal to the apparent power S. The proportional factor which links V_s and i_s together is the conductance g, which is calculated in the outer control loop and can also be calculated from the figure by utilizing (4.9).

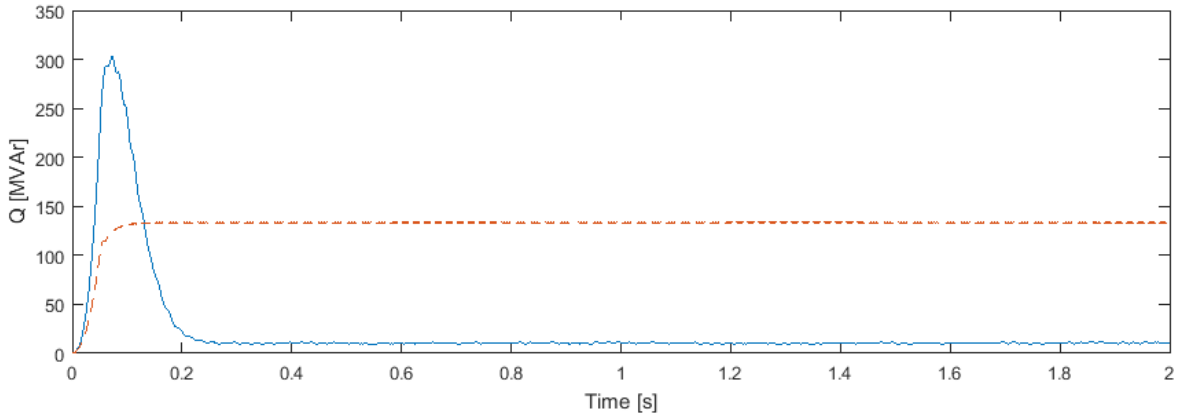

Figure 4.4: Active (P) and reactive power (Q). The dotted line is the reactive power supplied from source when the active filter is disabled.

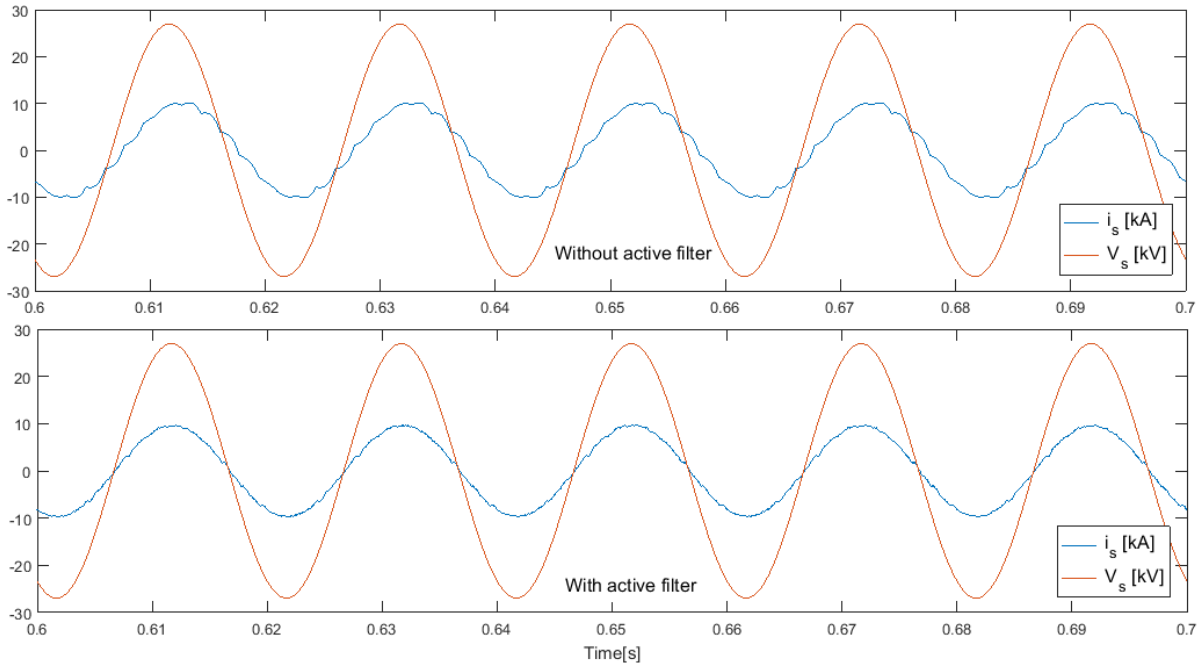

Figure 4.5: Source voltage and source current with and without APF.

4.6.3 Harmonic Compensation

Fig. 4.6 shows how the APF changes the shape of the active filter current i which is used to compensate for the selected harmonic components in the load current i_d, which can be observed in the second graph. It is observed that the upper graph, i, is more distorted when the harmonics are compensated by the filters and that the quality of the source current i_s is improved because the graph is less distorted. Fig. 4.7 shows the harmonic spectrum in the source current both with and without filter included in the controller. It can be observed that the filter has a great contribution in reducing the harmonic content. The THD of the source current is quantified and compared, which shows it reduces from 5% to 2% when the APF is included. The last graph shows that the source voltage is perfectly sinusoidal in both cases. This is because the voltage source represents a strong grid which is controlled by the WF, and it is not affected by the distorting load. Still, the THD can be reduced further by optimizing the filters, but the tuning is sufficient for the purpose of this report. The results prove that the APF controller is correctly designed and works sufficiently for the system with a balanced three-phased voltage and a distorted load.

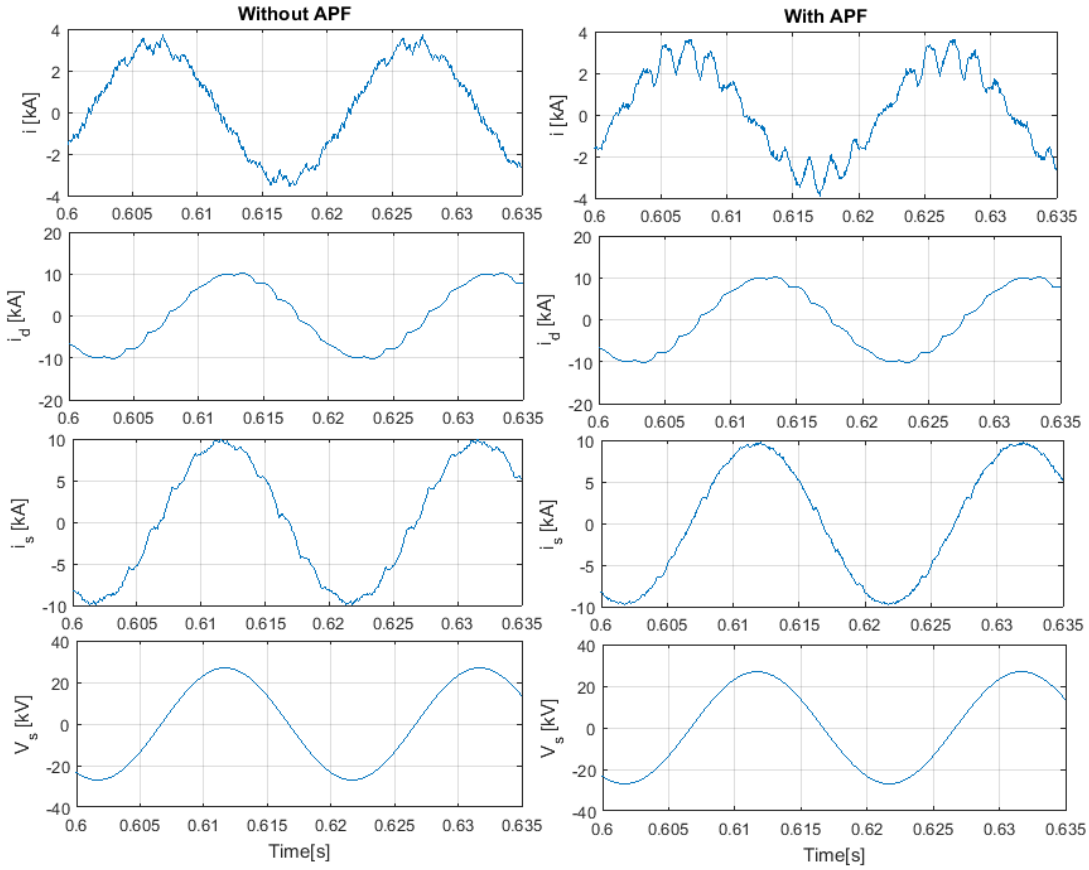

Figure 4.6: Influence of APF (from top to bottom): active filter current, load current, source current, source voltage. Left side is without APF compensation and the right side is with.

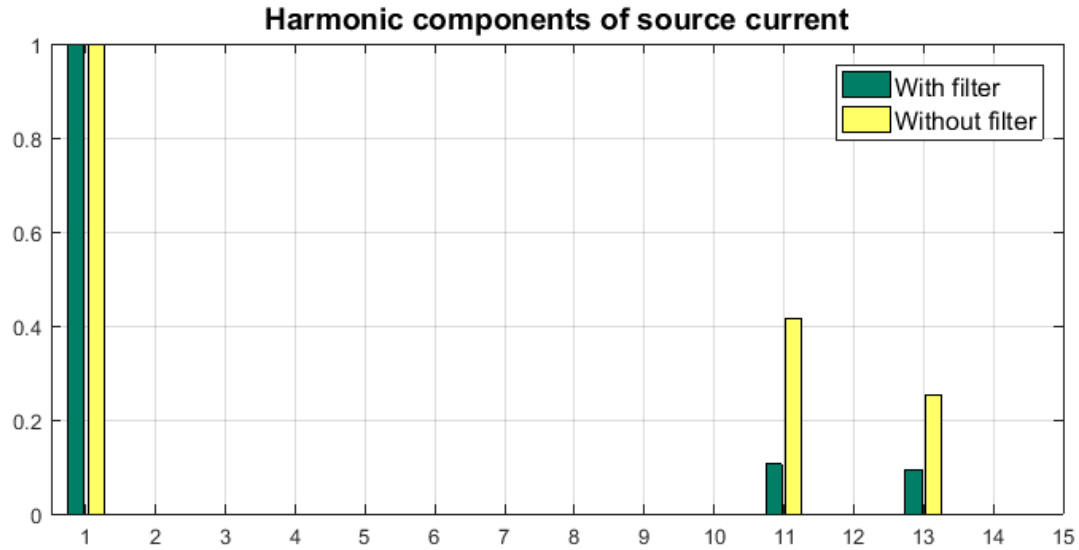

Figure 4.7: Harmonic spectrum in the source current of the APF topology.

4.6.4 DC Voltage Control

A PI controller is utilized to regulate the dc voltage in the simulations, but it can interfere with the natural power exchange [37]. This can lead to more distortion in $i^*_{s_{\alpha\beta}}$, thus a low-pass filter should be included in future work. Fig. 4.8 shows the dc voltage which is controlled by the APF. The dc voltage is regulated to the intended value with a fast response, which means that the controller is able to fulfill its control objective and it shows good performance.

Fig. 4.9 shows the conductance g which is calculated by the outer loop to be 0.35 S. The approximated pre-calculated value used in the inner loop design was calculated to be 0.367 S, which was very close to the actual value. This was a good estimation of g, and it proves that the simulation procedure was good.

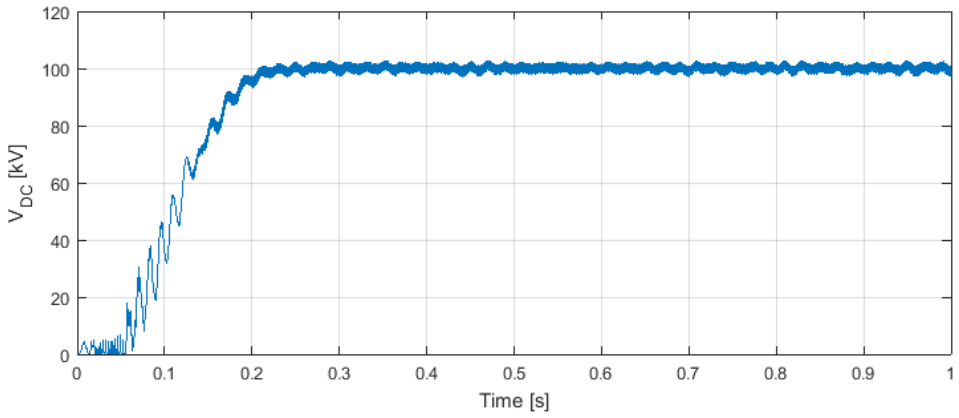

Figure 4.8: DC voltage controlled by active filter.

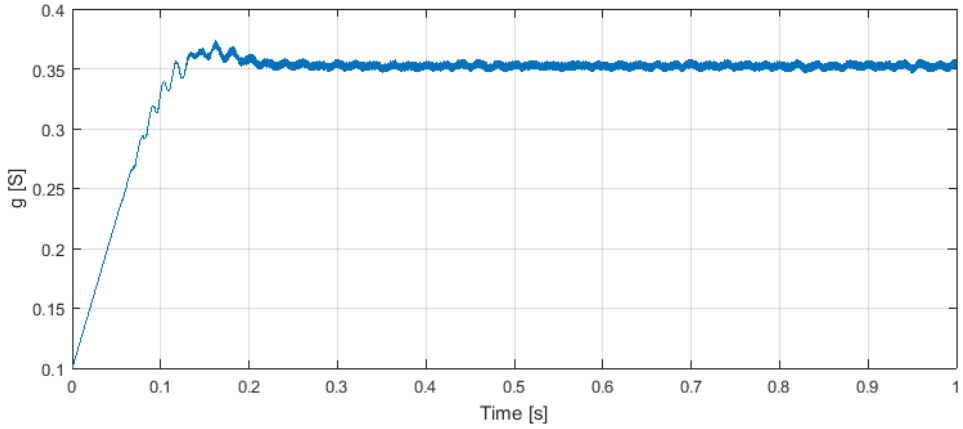

Figure 4.9: Calculated conductance g.

4.7 Discussion

Today, APFs are not applied to high power systems above 100 MVA because many expensive transistors are needed to withstand the high voltages and currents. But in Japan, several APFs in a range of 40 MVA to 60 MVA have been installed in substations along the Tokaido Shinkansen [11]. The APF can improve the power quality for some systems like the high-speed train and the offshore grid because it is flexible and adaptable, thus it will be able to eliminate all harmonics. The power electronic technology is continuously improved, thus the cost of APFs may reduce in time such that it can be beneficial to install in high power systems.

A trend in offshore HVDC transmission is to use a fully rated VSC on the offshore station because it is compact and has a smaller footprint compared to more traditional converter stations utilizing LCC. The alternative diode-based solution in this chapter has lower losses compared to the VSC-based solution because there are no switching losses. Other advantages of this solution are reduced cost and higher robustness of power electronic devices [9]. The security of power supply would be exposed in case of a fault in the switching controller of the VSC-based solution because the power transmission would not be possible. A diode-based solution will never have this problem and will, therefore, be more reliable because the diodes are uncontrollable.

A disadvantage of the uncontrollable DRs is the fact that the WF must modify its control objectives. The back-end converter of the WF needs to control the dc voltage such that the front-end converter can control the ac voltage of the offshore grid. A result of this alteration is that the FRC-WT will not be able to track the maximum power, thus some available power will be lost. Another disadvantage of using DRs is the great impact they have on the current waveform. The harmonics introduced by the DRs distort the current which will result in lower power quality.

The diode-based solution by Blasco et al. in [9] utilizes passive filters to eliminate the harmonics. The passive filters must be tuned to selected frequencies and can, unfortunately, be mistuned such that the harmonics are not fully compensated. Another drawback is the size of the passive filters in high power grids. The bulky filters are dependent on large offshore platforms which are problematic because of construction and

installation in deep water. The installation of large platforms in rough water will be costly and is a reason why a possible solution with an APF should be investigated.

The diode-based solution will become more compact when an APF is connected because it replaces the bulky filters. The size of the APF depends on the reactive current and the amount of reactive power that the DR needs [40]. The size of the APF will affect the total cost of the offshore platform because the more reactive power it must be able to deliver, the more expensive will the converter be. The optimal size can be found by calculating the reactive power needed and then how many transistors are needed. An optimal size and cost of the APF should be investigated in future work and then compared with the total cost of the other solutions.

Intuitively, one can conclude that the diode-based solution utilizing an APF will be a better solution than the fully rated VSC in offshore platforms at rough sea. This is because it is a robust and a relatively inexpensive solution, which will be compact because of the APF. But the size of the APF still needs to be calculated to find the total cost compared to the VSC-based solution. Another uncertainty is the effect of not being able to obtain maximum power extraction from because the control objective of the WF is altered. An assumption is that the wind quality is very good in the areas where this solution can be used, thus it is not necessary with power point tracking and it the power will not be lost. This is also a factor that must be investigated in future work.

An important drawback of the diode-based solution is the fact that it is not able to have a black start. A black start is described as the recovery after a complete system shutdown without an auxiliary power supply. Because the diode-based solution only has power flow in one direction, then this will not be possible and an auxiliary power supply is needed. The power supply will establish the voltage in the offshore grid before the power transfer can be enabled in the startup process.

The simulation results in this chapter showed that the APF controller works perfectly. The controller was able to provide both harmonic and reactive power compensation and the outer control loop showed a fast time response. These promising results were the reason why the PBC theory was applied when developing the controller for the hybrid topology in the next chapter.

4.8 Summary

The APF-DR topology has the advantage that it does not need passive filters like the DR-based solution does. Thus the space required on the offshore platform will be reduced which is an important factor for OWF development. The topology will also be more flexible and adaptable because it is controllable. The disadvantage compared to the VSC topology is that it can not control the power transfer, nor can it transfer power in both directions. The result of this is that the offshore platform needs an auxiliary power supply on the offshore platform for the startup process. This power supply requires space on the platform, which is a disadvantage.

The development of the passivity-based controller was studied in this chapter. A simulation procedure was described and the procedure for control parameter tuning was explained. A performance assessment of the controller for the APF showed that it was able to fulfill all control objectives and that it had a fast time response. The control theory explained in this chapter laid the foundation for further control design for a hybrid DR-VSC topology.

Chapter 5

Hybrid DR-VSC Topology

5.1 Introduction

The VSC in the hybrid converter topology has the same functions as the APF, which are compensation of reactive power and harmonic components in the grid voltage and current. Additionally, will the VSC be able to control the ac voltage in the offshore grid and convert a share of the active power. The design of the VSC controller in the hybrid topology is complex and an important engineering challenge because of all the functions the VSC must fulfill. The diode-based solution with the APF and the hybrid solution are based on the same components, but the arrangement makes a huge difference.

A control system for the hybrid model has been investigated in this chapter and different approaches have been tested to design the controller. In the end, some satisfying results have been obtained for a simplified model and a controller with simplified control objectives. The development and results of the hybrid controller will lay the foundation for further work on this topology, but this research is an important contribution to the search for an exciting new converter station which can improve the flexibility of OWFs.

5.2 Step by Step Method

The controller should be able to fulfill all three control objectives explained in Section 3.2.3. It is a challenge to implement such a complex controller, thus the controller should be built step by step. One step for each control objective:

1. Only voltage tracking control should be considered in the beginning. Thus, simple linear resistances can be used to represent the WF and the load, such that there will not be any disruptive sources. The transformer connected to the VSC can be neglected to simplify the model further, and the dc capacitor will be replaced by a dc voltage source to emulate the balancing control.
2. In the next step, the harmonic control must be implemented by including BPFs in the block diagram. The linear load will be replaced by a DR which introduces harmonics that must be eliminated by the BPFs.
3. In the last step, the dc voltage source will be replaced by a capacitor and the controller must be modified such that it will be able to provide the balancing control.

5.3 Double Loop Approach

The double loop controller is based on the cascaded controller concept, similar to the APF controller, where the current dynamics has a faster response than the dynamics of the capacitor [37]. As explained in the previous chapter, it is important to implement the model in a step by step method to make sure all parts work correctly. This is also done when designing the controller for the hybrid converter. Fig. 5.1 shows the simplified model for the first step and the system parameters are listed in Table 5.1.

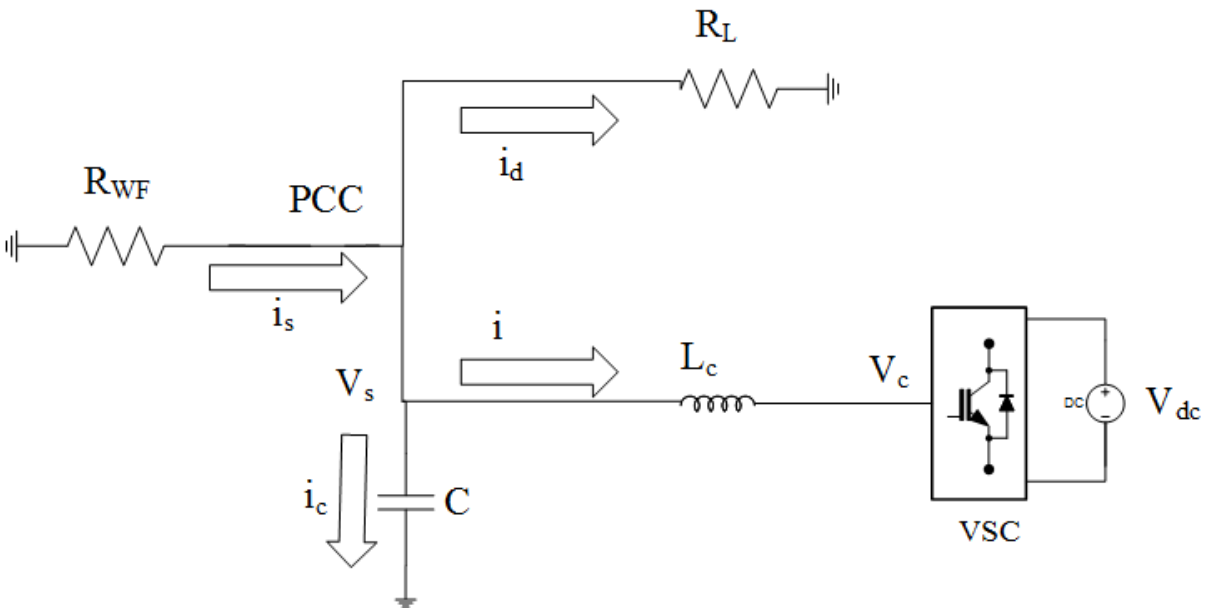

Figure 5.1: A simplified model for the double loop approach.

Table 5.1: System Parameters for Double Loop Approach

Power and Voltage	**Parameters**	**Values**	Unit
Base values	Power rating	400	MVA
	AC Voltage	33	kV
	DC Voltage	100	kV
	frequency	50	Hz
Passive elements			
	C	3	μF
	L_c	45	mH
	R_L	11.34	Ω
	R_{WF}	10	Ω

5.3.1 Control Design

The design of the double loop controller is based on the controller in [37], and on the system equations derived from Fig. 5.1. Equation (5.1) is derived by applying KVL to the system and (5.2) by applying Kirchhoff's Current Law (KCL):

$$L_c \frac{d\boldsymbol{i}(\boldsymbol{t})}{dt} = \boldsymbol{V_s}(\boldsymbol{t}) - \boldsymbol{V_c}(\boldsymbol{t}) \tag{5.1}$$

$$C \frac{d\boldsymbol{V_s}(\boldsymbol{t})}{dt} = \boldsymbol{i_s}(\boldsymbol{t}) - \boldsymbol{i_d}(\boldsymbol{t}) - \boldsymbol{i}(\boldsymbol{t}) = \boldsymbol{i_c}(\boldsymbol{t}) \tag{5.2}$$

where the inductor resistance is neglected because it only adds damping to the system. The grid voltage, $\boldsymbol{V_s}(\boldsymbol{t})$, input converter voltage, $\boldsymbol{V_c}(\boldsymbol{t})$ and phase currents, ($\boldsymbol{i}(\boldsymbol{t})$, $\boldsymbol{i_d}(\boldsymbol{t})$, $\boldsymbol{i_s}(\boldsymbol{t})$, $\boldsymbol{i_c}(\boldsymbol{t})$) are given as balanced three-phase vectors $\boldsymbol{X} = [X_a \quad X_b \quad X_c]^T$.

For control purposes it is useful to express the control currents $\boldsymbol{i}(\boldsymbol{t})$ in terms of the source currents $\boldsymbol{i_s}(\boldsymbol{t})$ in (5.1):

$$\boldsymbol{i}(\boldsymbol{t}) = \boldsymbol{i_s}(\boldsymbol{t}) - \boldsymbol{i_d}(\boldsymbol{t}) - \boldsymbol{i_c}(\boldsymbol{t}).$$

Clarke transformation from Appendix B is applied to the system equations and the resulting system in stationary reference frame becomes:

$$L_c \frac{di s_{\alpha\beta}}{dt} = V_{s_{\alpha\beta}} - V_{c_{\alpha\beta}} + L_c \frac{di_{d_{\alpha\beta}}}{dt} + L_c \frac{di_{c_{\alpha\beta}}}{dt} \tag{5.3}$$

$$C \frac{dV_{s_{\alpha\beta}}}{dt} = i_{s_{\alpha\beta}} - i_{d_{\alpha\beta}} - i_{\alpha\beta}. \tag{5.4}$$

where $i_{s_{\alpha\beta}} = [i_{s_\alpha} i_{s_\beta}]^T, i_{d_{\alpha\beta}} = [i_{d_\alpha} i_{d_\beta}]^T, V_{s_{\alpha\beta}} = [V_{s_\alpha} V_{s_\beta}]^T$ etc.

Because the current dynamics in the system equations are assumed to be much faster than the dynamics involving the capacitor, the control design can be simplified by splitting it into two stages: current (inner loop) and voltage (outer loop) control design.

Inner Loop

The first step in control design is to develop the inner control loop [41]. In the known parameter case, the ideas from the ESDI design technique [32] are applied to the system. First, the damping injection stage is performed where the state $i_{s_{\alpha\beta}}$ in (5.3) is replaced by $i^*_{s_{\alpha\beta}}$ and a damping term is added

$$L_c \frac{di^*_{s_{\alpha\beta}}}{dt} = V_{s_{\alpha\beta}} - V_{c_{\alpha\beta}} + L_c \frac{di_{d_{\alpha\beta}}}{dt} + L_c \frac{di_{c_{\alpha\beta}}}{dt} + K_1 \tilde{i}_{s_{\alpha\beta}} \tag{5.5}$$

where $\tilde{i}_{s_{\alpha\beta}} \triangleq i_{s_{\alpha\beta}} - i^*_{s_{\alpha\beta}}$ and K_1 is a positive-definite design matrix, used to introduce the required damping.

Equation (5.5) is solved for the controlling parameter and gives

$$V_{c_{\alpha\beta}} = V_{s_{\alpha\beta}} - L_c \frac{di^*_{s_{\alpha\beta}}}{dt} + L_c \frac{di_{d_{\alpha\beta}}}{dt} + L_c \frac{di_{c_{\alpha\beta}}}{dt} + K_1 \tilde{i}_{s_{\alpha\beta}}. \tag{5.6}$$

Equation (5.6) substituted in (5.3) gives the differential equation $L_c \frac{d\tilde{i}_{s_{\alpha\beta}}}{dt} = -K_1 \tilde{i}_{s_{\alpha\beta}}$. The solution to this differential equation is $\tilde{i}_{s_{\alpha\beta}} = e^{\frac{-K_1}{L}t}$, which becomes zero when $t \to \infty$. Hence, the inner control loop will fulfill its control objective which is to track the reference current $i^*_{s_{\alpha\beta}}$.

Outer Loop

The same damping injection technique which is applied to the inner loop is also utilized when designing the outer control loop. By assuming $V_{s_{\alpha\beta}} = V^*_{s_{\alpha\beta}}$ in (5.4) and adding a damping term, (5.7) is achieved.

$$C \frac{dV^*_{s_{\alpha\beta}}}{dt} = i^*_{s_{\alpha\beta}} - i_{d_{\alpha\beta}} - i_{\alpha\beta} + K_2 \tilde{V}_{s_{\alpha\beta}} \tag{5.7}$$

where the assumption $i_{s_{\alpha\beta}} = i^*_{s_{\alpha\beta}}$ still counts and $\tilde{V}_{s_{\alpha\beta}} \triangleq V_{s_{\alpha\beta}} - V^*_{s_{\alpha\beta}}$. K_2 is a positive-definite design matrix used to introduce the required damping.

Equation (5.7) is solved for the controlling parameter and gives

$$i^*_{s_{\alpha\beta}} = C\frac{dV^*_{s_{\alpha\beta}}}{dt} - K_2\tilde{V}_{s_{\alpha\beta}} + i_{d_{\alpha\beta}} + i_{\alpha\beta}. \tag{5.8}$$

Controller (5.8) is substituted in (5.4) and the differential equation is solved and the solution shows that when $t \to \infty$, $\tilde{V}_{s_{\alpha\beta}} \to 0$.

Resulting Controller

The time derivative of the reference source voltage, which is defined in (3.2), will in a balanced system be $\frac{dV^*_{s_{\alpha\beta}}}{dt} = \boldsymbol{J}\omega V^*_{s_{\alpha\beta}}$. For the double loop approach, it is assumed that the system is balanced such that the time derivative of the source voltage can be applied. The time derivative terms of the currents in (5.6) will contain harmonic content when the 12P-DR is connected as a load, thus they can not be calculated in a straightforward manner. All the harmonic coefficients are lumped together in an unknown parameter $\hat{\phi}$ as described for the controller in Section 4.3. Because the distorted load is replaced by a linear resistance in the first implementation, it is assumed that the lumped parameter $\hat{\phi}$ can be neglected. The resulting block diagram is shown in Fig. 5.2.

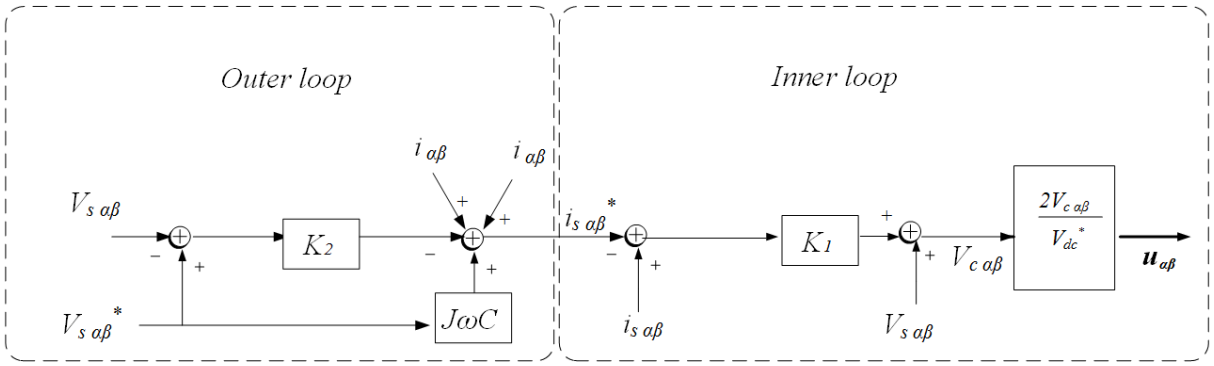

Figure 5.2: Block diagram for the double loop approach without harmonic control.

5.3.2 Implementation in PSCAD

The double loop controller was implemented in PSCAD and first tested for the linear load with parameter K_1 and K_2 equal to 30 and 2, respectively. The controller was able to track the reference as shown in Fig. 5.3. The per unit representation was used to implement the

controller in PSCAD, thus 1 $p.u.$ peak value was used as reference voltage as seen in the figure.

The controller was only proven to be valid for linear loads. For harmonic loads, the controller was not able to eliminate the harmonics when the harmonic control was included. The reason was that the measured signal V_s introduced in the inner loop reduced the effect of the filter. A single loop controller was developed due to this discovery.

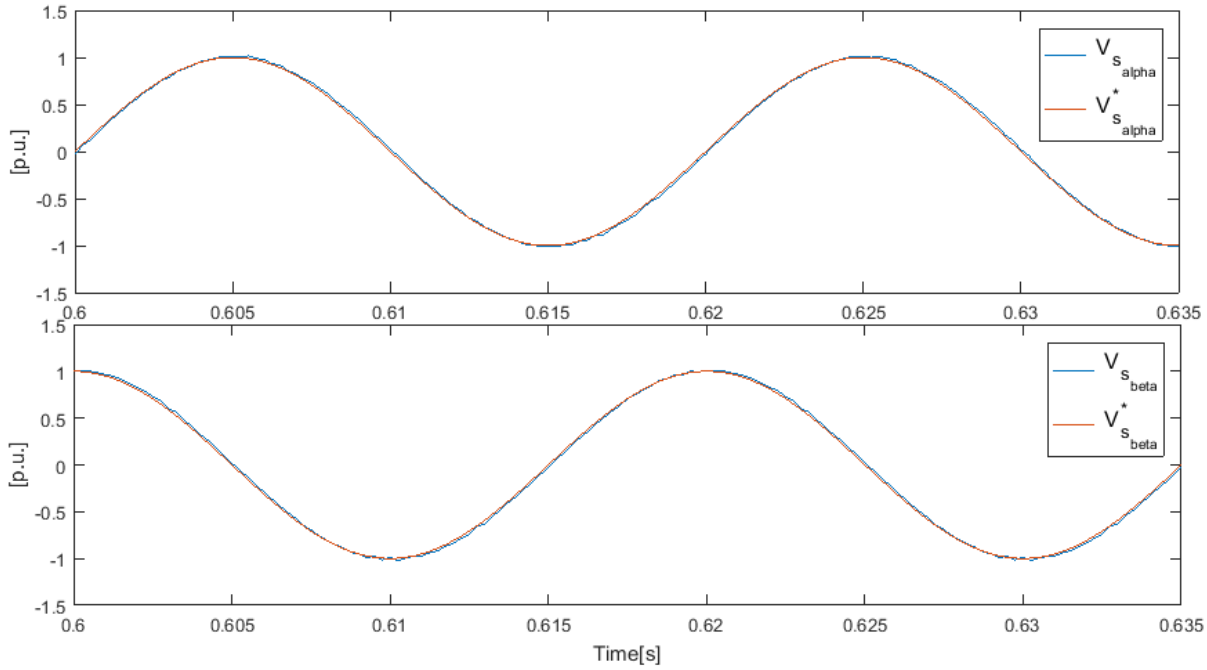

Figure 5.3: Voltage tracking for double loop approach with the linear load.

5.4 Single Loop Approach

The development of the single loop controller was done in a step by step method where Fig. 5.4 shows the implementation of the first step in PSCAD. In the first step the VSC was connected to a linear load, and in the second step, the VSC was connected to a 12P-DR as shown in Fig. 5.5. Table 5.2 shows the system parameters used in the simulations.

5.4.1 Control Design

The control design was developed based on the system equations derived from Fig. 5.4 and the passivity-based control theory from Section 3.6. The average system equations were

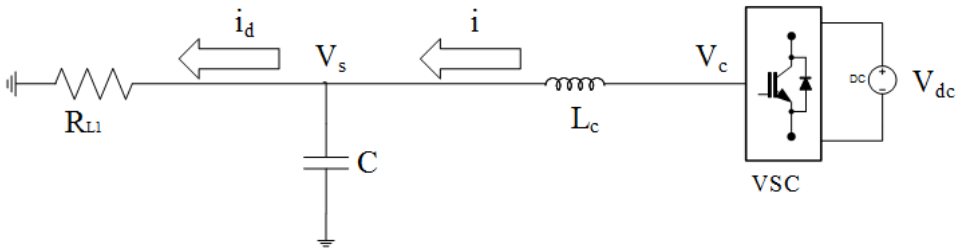

Figure 5.4: First step implementation: voltage tracking control.

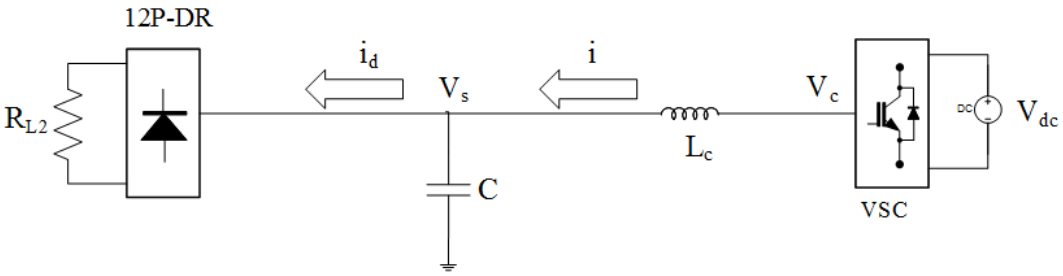

Figure 5.5: Second step implementation: harmonic control.

Table 5.2: System Parameters for Single Loop Approach

Power and Voltage	**Parameters**	**Values**	Unit
Base values	Power rating	400	MVA
	AC Voltage	33	kV
	DC Voltage	100	kV
	frequency	50	Hz
Passive elements			
	C	48.7	μF
	L_c	13	mH
	R_{L1}	2.72	Ω
	R_{L2}	100	Ω

derived and transformed into the stationary reference frame:

$$\begin{aligned} L_c \frac{di_{\alpha\beta}}{dt} &= -V_{s_{\alpha\beta}} + \frac{V_{dc}}{2} u_{\alpha\beta} \\ C \frac{dV_{s_{\alpha\beta}}}{dt} &= i_{\alpha\beta} - i_{d_{\alpha\beta}} \end{aligned} \tag{5.9}$$

where $V_{c_{\alpha\beta}} = \frac{V_{dc}}{2} u_{\alpha\beta}$ was applied, and $\boldsymbol{u}$ is the duty ratio in the average model.

The control objective of the voltage tracking control is to force $\boldsymbol{V}_s^* = e^{\boldsymbol{J}\omega t}[V_s, 0]^T$, which is a

balanced sinusoidal vector signal. The equilibrium point for the system (5.9) becomes

$$\bar{i}_{\alpha\beta} = i_{d_{\alpha\beta}} + \boldsymbol{J}\omega C V^*_{s_{\alpha\beta}} \tag{5.10}$$

where the notation $\overline{(.)}$ denotes values in equilibrium. The fact that $\frac{dV^*_{s_{\alpha\beta}}}{dt} = \boldsymbol{J}\omega V^*_{s_{\alpha\beta}}$ at the equilibrium point is applied. It can be seen from (5.10) that the converter current $i_{\alpha\beta}$ must provide the harmonic content of the load current $i_{d_{\alpha\beta}}$ when the 12P-DR is connected. Thus a harmonic filter bank must be included in the second step of the control design procedure.

The error model of the system (5.9) is

$$\begin{aligned} L_c\frac{d\tilde{i}_{\alpha\beta}}{dt} &= -\tilde{V}_{s_{\alpha\beta}} - V^*_{s_{\alpha\beta}} + \frac{V_{dc}}{2}u_{\alpha\beta} - L_c\frac{d\bar{i}_{\alpha\beta}}{dt} \\ C\frac{d\tilde{V}_{s_{\alpha\beta}}}{dt} &= \tilde{i}_{\alpha\beta} + \bar{i}_{\alpha\beta} - i_{d_{\alpha\beta}} + \boldsymbol{J}\omega V^*_{s_{\alpha\beta}} = \tilde{i}_{\alpha\beta} \end{aligned} \tag{5.11}$$

where $\tilde{i}_{\alpha\beta} \triangleq i_{\alpha\beta} - \bar{i}_{\alpha\beta}$ and $\tilde{V}_{s_{\alpha\beta}} \triangleq V_{s_{\alpha\beta}} - V^*_{s_{\alpha\beta}}$. The fact that $i^*_{\alpha\beta} = \bar{i}_{\alpha\beta}$ is applied for the equilibrium point.

A controller for the known parameter case is developed based on the ESDI technique [32]:

1. Two design parameters K_1 and K_2 are included to add damping to the system. The controller which guarantees perfect voltage tracking, i.e. $\tilde{V}_{s_{\alpha\beta}} \to 0$ and $\tilde{i}_{\alpha\beta} \to 0$, is

$$\frac{V_{dc}}{2}u_{\alpha\beta} = -K_1(i_{\alpha\beta} - \bar{i}_{\alpha\beta}) - K_2\tilde{V}_{s_{\alpha\beta}} + V^*_{s_{\alpha\beta}} + L_c\frac{d\bar{i}_{\alpha\beta}}{dt}. \tag{5.12}$$

2. The parameter $\bar{i}_{\alpha\beta}$ in (5.12) is an unknown and distorted signal and the terms including this parameter are lumped together into one parameter $\hat{\phi}_k$ and the resulting controller is as follows:

$$\frac{V_{dc}}{2}u_{\alpha\beta} = -K_1 i_{\alpha\beta} - K_2\tilde{V}_{s_{\alpha\beta}} + V^*_{s_{\alpha\beta}} + \hat{\phi}_k \tag{5.13}$$

where $\hat{\phi} \triangleq K_1\bar{i}_{\alpha\beta} + L_c\frac{d\bar{i}_{\alpha\beta}}{dt}$.

Controller (5.13) applied to error model (5.11) gives the system

$$L_c\frac{d\tilde{i}_{\alpha\beta}}{dt} = -K_1(\tilde{i}_{\alpha\beta}+\overline{i}_{\alpha\beta}) - (1+K_2)\tilde{V}_{s_{\alpha\beta}} + \hat{\phi}_k - L_c\frac{d\overline{i}_{\alpha\beta}}{dt}$$
$$= -K_1\tilde{i}_{\alpha\beta} - (1+K_2)\tilde{V}_{s_{\alpha\beta}} + \tilde{\phi} \tag{5.14}$$
$$C\frac{d\tilde{V}_{s_{\alpha\beta}}}{dt} = \tilde{i}_{\alpha\beta} \tag{5.15}$$

where $\tilde{\phi} \triangleq \hat{\phi} - \overline{\phi}$ and $\overline{\phi} \triangleq K_1\overline{\phi} + L_c\frac{d\overline{i}_{\alpha\beta}}{dt}$. The periodic disturbance $\tilde{\phi}$ is defined as

$$\tilde{\phi} = \sum_{k\in\chi}\left(\tilde{\phi}_k^p + \tilde{\phi}_k^n\right) = \sum_{k\in\chi}\left(e^{\boldsymbol{J}k\omega t}\tilde{\Phi}_k^p + e^{-\boldsymbol{J}k\omega t}\tilde{\Phi}_k^n\right) \tag{5.16}$$

and is given in $\alpha\beta$-coordinates. $\tilde{\Phi}_k^p, \tilde{\Phi}_k^n$ are the parameter errors of the kth harmonic coefficient for the positive and negative sequence representation of the distortion $\tilde{\phi}$.

The parameter errors can be represented by adaptive laws, which are developed by following the Lyapunov approach [32]:

1. First, a Lyapunov equation W, fulfilling the characteristics presented in Section 3.6, is proposed

$$W = \frac{L_c C|\dot{\tilde{V}}_{s_{\alpha\beta}}|^2}{2} + \frac{(1+K_2)|\tilde{V}_{s_{\alpha\beta}}|^2}{2} + \sum_{k\in\chi}\frac{1}{2\gamma_k}\left[(\tilde{\Phi}_k^p)^2 + (\tilde{\Phi}_k^n)^2\right] \tag{5.17}$$

where the notation $|(.)|$ indicates the module of the parameter, thus $|X|^2 = X^T X$.

2. The second step is to find the derivative of the Lyapunov equation along the trajectories of the error model (5.14),(5.15). The chain rule is applied to each part of

the Lyapunov equation as follows:

$$\Big(\frac{L_c C|\dot{\tilde{V}}_{s_{\alpha\beta}}|^2}{2}\Big)' = L_c C\dot{\tilde{V}}_{s_{\alpha\beta}}^T \frac{\dot{\tilde{i}}_{m_{\alpha\beta}}}{C} = \dot{\tilde{V}}_{s_{\alpha\beta}}^T L_c \dot{\tilde{i}}_{m_{\alpha\beta}}$$

Equation (5.14) and (5.15) are applied:

$$= -\dot{\tilde{V}}_{s_{\alpha\beta}}^T (1+K_2)\tilde{V}_{s_{\alpha\beta}} - \dot{\tilde{V}}_{s_{\alpha\beta}}^T K_1 C\dot{\tilde{V}}_{s_{\alpha\beta}} + \dot{\tilde{V}}_{s_{\alpha\beta}}^T \sum_{k\in\chi}\Big(e^{\boldsymbol{J}k\omega t}\tilde{\Phi}_k^p + e^{-\boldsymbol{J}k\omega t}\tilde{\Phi}_k^n\Big)$$

$$\Big(\frac{(1+K_2)|\tilde{V}_{s_{\alpha\beta}}|^2}{2}\Big)' = \dot{\tilde{V}}_{s_{\alpha\beta}}^T (1+K_2)\tilde{V}_{s_{\alpha\beta}}$$

$$\Big(\sum_{k\in\chi}\frac{1}{2\gamma_k}\Big[(\tilde{\phi}_k^p)^2 + (\tilde{\phi}_k^n)^2\Big]\Big)' = \sum_{k\in\chi}\frac{1}{\gamma_k}\Big[(\dot{\tilde{\phi}}_k^p)^T\tilde{\phi}_k^p + (\dot{\tilde{\phi}}_k^n)^T\tilde{\phi}_k^n\Big]$$

Adding all terms together gives final expression:

$$\dot{W} = -K_1 C\dot{\tilde{V}}_{s_{\alpha\beta}}^2 + \dot{\tilde{V}}_{s_{\alpha\beta}}^T \sum_{k\in\chi}\Big(e^{\boldsymbol{J}k\omega t}\tilde{\Phi}_k^p + e^{-\boldsymbol{J}k\omega t}\tilde{\Phi}_k^n\Big) + \sum_{k\in\chi}\frac{1}{\gamma_k}\Big[(\dot{\tilde{\Phi}}_k^p)^T\tilde{\Phi}_k^p + (\dot{\tilde{\Phi}}_k^n)^T\tilde{\Phi}_k^n\Big].$$

3. The derivative is made negative semidefinite by utilizing the adaption laws:

$$\dot{\tilde{\Phi}}_k^p = -\gamma_k e^{-\boldsymbol{J}k\omega t}\dot{\tilde{V}}_{s_{\alpha\beta}} \quad \dot{\tilde{\Phi}}_k^n = -\gamma_k e^{\boldsymbol{J}k\omega t}\dot{\tilde{V}}_{s_{\alpha\beta}}$$

where the fact that $\dot{\hat{\Phi}}_k^p = \dot{\tilde{\Phi}}_k^p$ and $\dot{\hat{\Phi}}_k^n = \dot{\tilde{\Phi}}_k^n$ are applied since Φ_k^p and Φ_k^n are assumed to be constants. The derivative becomes

$$\dot{W} = -K_1 C\dot{\tilde{V}}_{s_{\alpha\beta}}^2$$

which is a negative semidefinite function. Two important conclusions can be drawn from this:

(a) The voltage tracking control is fulfilled because $\tilde{V}_{s_{\alpha\beta}} \to 0$ when $t \to \infty$.

(b) The harmonic control is fulfilled because $\tilde{\phi}_k \to 0$ when $t \to \infty$.

4. The adaptive laws are transformed into a representation which can be implemented in the controller. The transformation utilized is

$$\hat{\phi}_k^p = e^{\boldsymbol{J}k\omega t}\hat{\Phi}_k^p \quad \hat{\phi}_k^n = e^{-\boldsymbol{J}k\omega t}\hat{\Phi}_k^n$$

and the resulting adaptive laws are

$$\dot{\hat{\phi}}_k^p = -\gamma_k \dot{\tilde{V}}_{s_{\alpha\beta}} + \boldsymbol{J}k\omega\hat{\phi}_k^p \quad \dot{\hat{\phi}}_k^n = -\gamma_k \dot{\tilde{V}}_{s_{\alpha\beta}} - \boldsymbol{J}k\omega\hat{\phi}_k^n$$
$$s\hat{\phi}_k^p = -\gamma_k s\tilde{V}_{s_{\alpha\beta}} + \boldsymbol{J}k\omega\hat{\phi}_k^p$$
$$\hat{\phi}_k^p = \frac{-\gamma_k s(s+\boldsymbol{J}k\omega)}{s^2+k^2\omega^2}\tilde{V}_{s_{\alpha\beta}}$$
$$\hat{\phi}_k^n = \frac{-\gamma_k s(s-\boldsymbol{J}k\omega)}{s^2+k^2\omega^2}\tilde{V}_{s_{\alpha\beta}}$$

where s is the complex variable in the Laplace transformation. The sum of the positive and negative sequence component is

$$\begin{aligned}\hat{\phi}_k = \hat{\phi}_k^p + \hat{\phi}_k^n &= \frac{-2\gamma_k s^2}{s^2+k^2\omega^2}\tilde{V}_{s_{\alpha\beta}} \\ &= -2\gamma_k\tilde{V}_{s_{\alpha\beta}} + \frac{2\gamma_k k^2\omega^2}{s^2+k^2\omega^2}\tilde{V}_{s_{\alpha\beta}}\end{aligned} \tag{5.18}$$

Equation (5.18) in controller (5.13) gives the final expression for the controller:

$$\frac{V_{dc}}{2}u_{\alpha\beta} = -K_1 i_{\alpha\beta} - (K_2 + 2\sum_{k\in\chi}\gamma_k)\tilde{V}_{s_{\alpha\beta}} + V^*_{s_{\alpha\beta}} + \frac{2\gamma_k k^2\omega^2}{s^2+k^2\omega^2}\tilde{V}_{s_{\alpha\beta}} \tag{5.19}$$

The bank of resonant filters, $\frac{2\gamma_k k^2\omega^2}{s^2+k^2\omega^2}\tilde{V}_{s_{\alpha\beta}}$, will make sure that the VSC can act as an active filter to eliminate the harmonic current components. The resonant filter banks are replaced by BPFs to limit the gain at resonant frequency [42]. The transfer function is presented in (5.20) for the BPF, where v_o, v_i are the output and input signals of the filters, respectively.

$$\frac{v_o}{v_i} = \frac{2\gamma_k k^2\omega_0^2}{s^2 + sk\omega/Q_k + k^2\omega^2} \tag{5.20}$$

where Q_k is the quality factor of the kth BPF.

Fig. 5.6 shows the controller for the first implementation in PSCAD for voltage tracking control where the lumped parameter $\hat{\phi}_k$ is neglected. Fig. 5.7 shows the controller for the second implementation when both voltage tracking control and harmonic control were tested. The proportional controller in Fig. 5.7 is $A = K_2 + 2\sum_{k\in\chi}\gamma_k$.

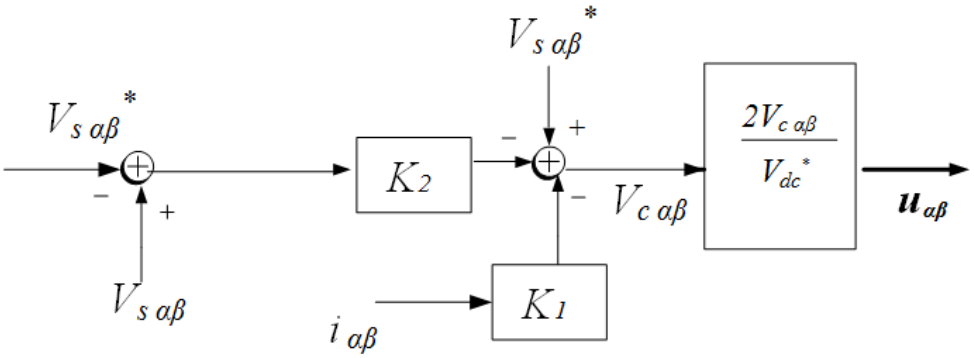

Figure 5.6: Proposed controller for voltage tracking.

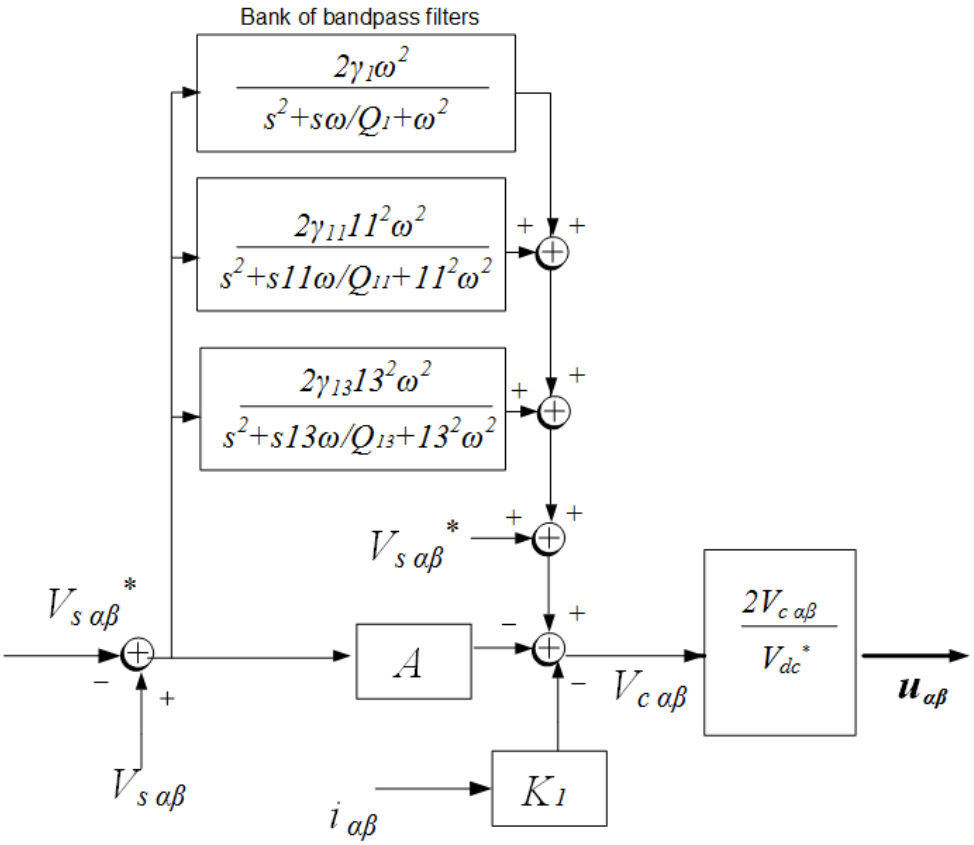

Figure 5.7: Proposed controller for voltage tracking and harmonic control.

5.4.2 Simulation Procedure

The testing of the controller was done in a step by step method as explained earlier, which was as follows:

1. In the beginning, only a linear resistance was connected to the VSC and there were no harmonics distorting the current. Only the voltage tracking control was implemented, thus the lumped parameter was neglected as seen in the control diagram in Fig. 5.2.
2. The 12P-DR, which produce the 11th- and the 13th order harmonic components in the current, replaced the linear resistance and the BPFs were included as seen in control diagram in Fig. 5.7.
3. The last step, which is to implement the balancing control, was not performed for the single loop controller in this thesis because of time restrictions. This is work for the future.

5.4.3 Results

First Step: Voltage Tracking Control

In the first step, the system model from Fig. 5.4 and controller from Fig. 5.6 were implemented. The controller was tuned by trial and error method until the error in $\alpha\beta$-coordinates was almost zero and values for K_1 and K_2 were obtained. The proportional controller was able to eliminate the phase shift between the reference value and the measured value as seen in Fig. 5.8. It can be observed in Fig. 5.9 that controller was able to track the reference voltage at 33 kV when the control parameters were tuned. It was concluded that the voltage tracking controller was working as it was supposed to, and the next step in the process was commenced.

Table 5.3: Control Parameters for Hybrid controller

Parameter	Value	Parameter	Value
Proportional Controller			
K_1	1	K_2	4
BPF			
γ_1	0.001	Q_1	0.1
$\gamma_1 1$	0.0001	$Q_1 1$	0.1
$\gamma_1 3$	0.00001	$Q_1 3$	0.1

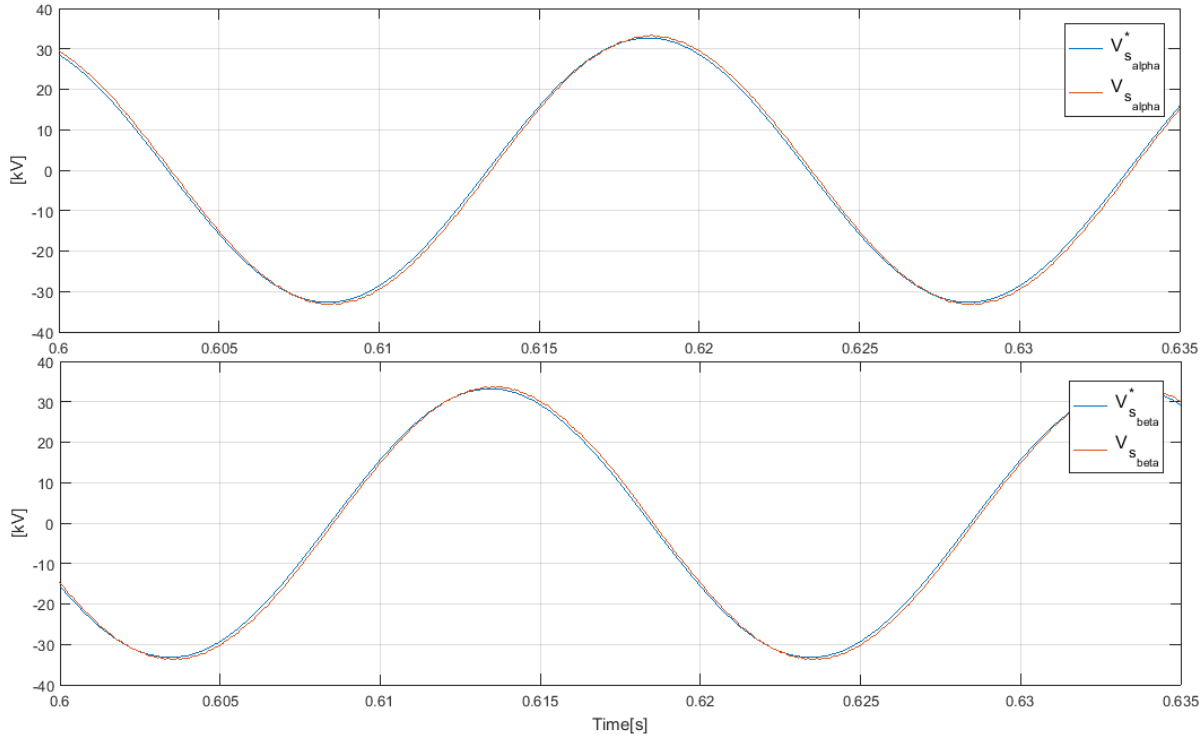

Figure 5.8: Voltage tracking control in $\alpha\beta$-coordinates for the simplified system with only a linear load.

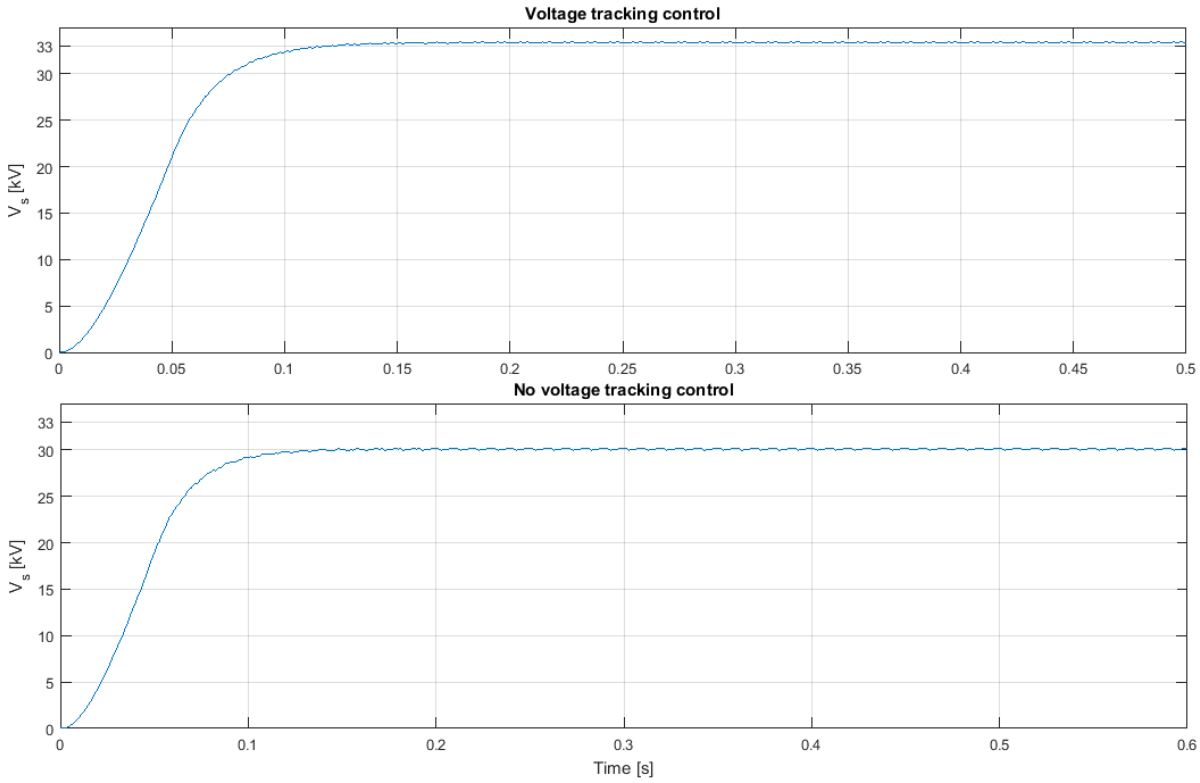

Figure 5.9: Measured source voltage V_s (LL). First graph when design parameter K_1 and K_2 are tuned, and second graph when they are not tuned.

Second Step: Harmonic Control

In the second step, the 12P-DR was included and it can be seen from Fig. 5.11 that the 11th- and 13th- order harmonic components of the source voltage must be compensated by the converter. The filters were included one by one and tuned by the trial and error-method, and the final parameters can be found in Table 5.3.

It was expected that the harmonic voltage components were eliminated when the filters were included, which was not the case as seen in Fig. 5.10. It was observed in Fig. 5.11 that the harmonic components increased. The THD increased from 14.23% to 14.98% when the filters were included, which indicates that the controller is limited to linear loads. Harmonic and balancing control for this hybrid controller remains for future work because time restrictions prevented the work from continuing. A good indicator that the controller will work in the future is that a similar controller is working for the APF-DR topology.

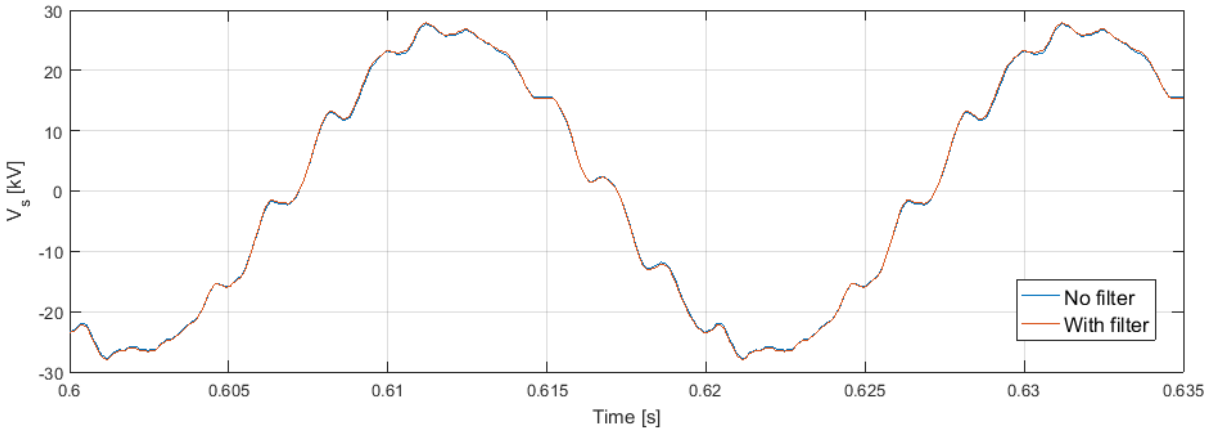

Figure 5.10: Source voltage V_s when 12P-DR is used as a load.

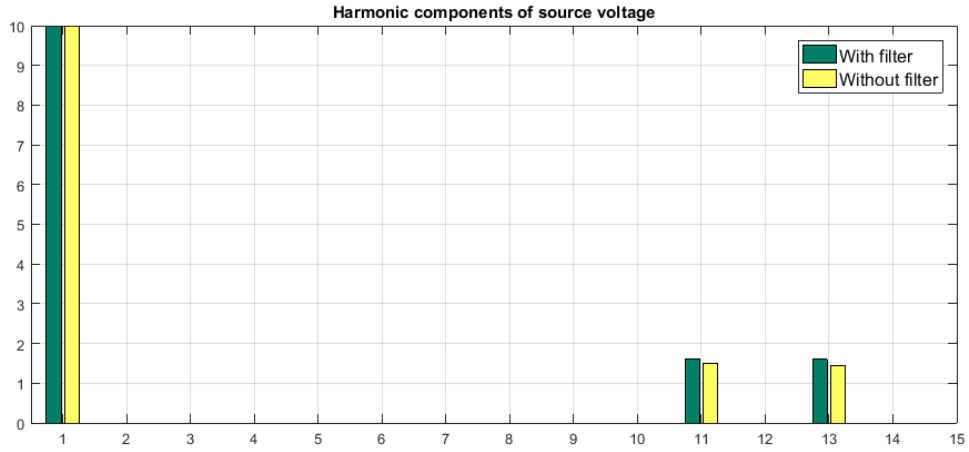

Figure 5.11: Harmonic spectrum of the source voltage.

5.5 APF Approach

The controller applied for the APF-DR topology was implemented for the hybrid topology to show that the PBC design will also work for the hybrid topology. The APF approach utilizes a simplified system and the control objectives are not as complex as the previous controllers, due to the elimination of voltage tracking control. The hybrid system consists of the same components as the APF topology in Fig. 4.1, but the difference between the two topologies is the way the VSC is connected to the 12P-DR. The VSC is connected in series with the 12P-DR in the hybrid topology, and in shunt for the APF topology.

The power transfer through the HVDC link is emulated by utilizing a linear load R_L in the simulation, which is connected to the dc side. The resistance dictates the power transfer artificially, and is calculated as $R_L = \frac{V^2}{P}$. System parameters used in the simulation are given in Table 5.4 and the system topology is shown in Fig. 5.12.

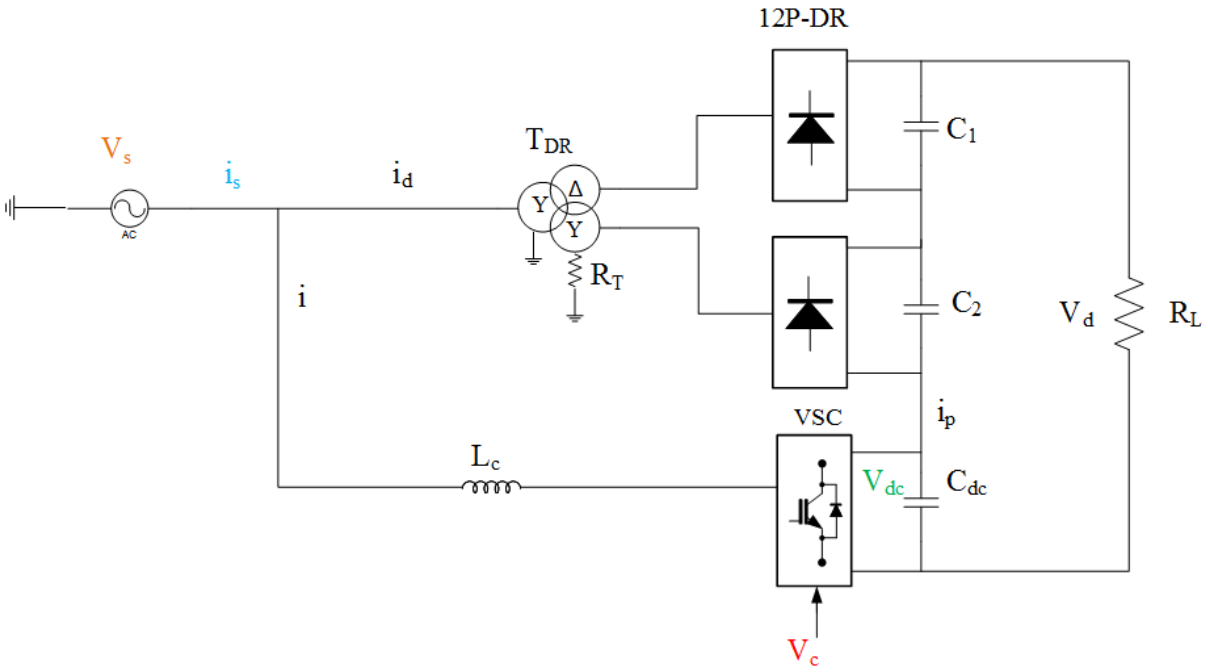

Figure 5.12: Single-line diagram for the hybrid DR-VSC topology.

Table 5.4: System Parameters for APF Approach

Power and Voltage	**Parameters**	**Values**	Unit
Base values	Power rating	400	MVA
	AC Voltage	33	kV
	frequency	50	Hz
Passive elements	C_1	300	μF
	C_2	300	μF
	C_{dc}	300	μF
	L_c	13	mH
	R_L	225	Ω
	R_T	1	MΩ
Transformer	T_{DR}	33/76/76	kV
	X_T	0.1	p.u.

5.5.1 Control Design

The ac voltage is controlled by the WF, thus the remaining control objectives for the VSC are harmonic control and balancing control which are the same control objectives as for the APF. In the APF approach, the APF controller from Section 4.3 was tested for the hybrid topology. The same control parameters, shown in Table 4.2, was utilized.

A simple block diagram of the controller is shown in Fig. 5.13, and the color-code which is used on the measured control parameters can also be found in Fig. 5.12.

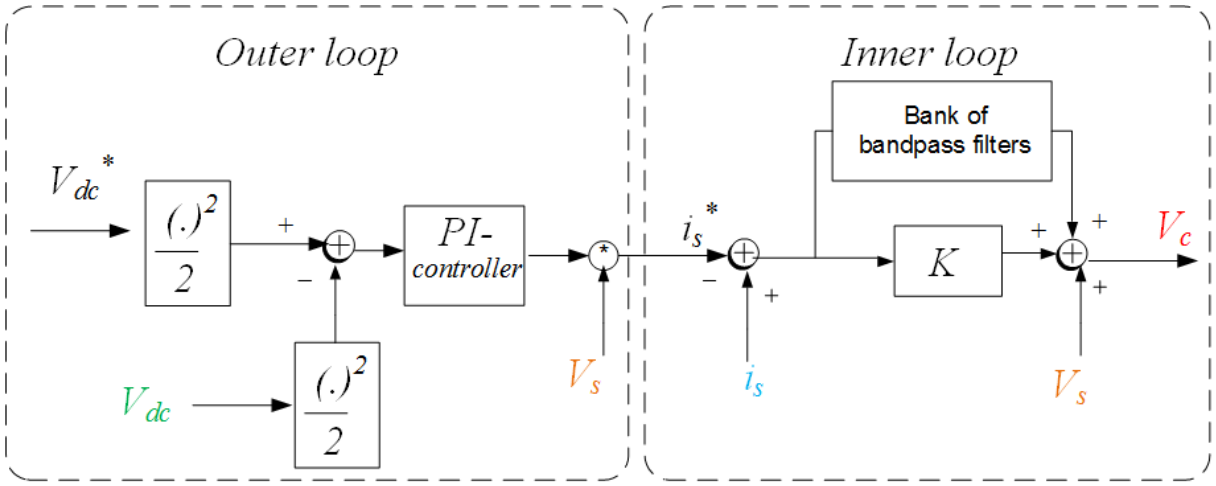

Figure 5.13: Block diagram for the controller [adapted from][37].

5.5.2 Results

Controller Analysis

One of the control objectives for the hybrid topology was the balancing control, which made sure the dc voltage between the 12P-DR and the VSC were balanced. This was previously ensured by utilizing a dc voltage source, but for the APF approach, the dc voltage over a capacitor is controlled to a predefined reference value. Fig. 5.14 shows the control response when the reference was set to 100 kV after 0.2 sec. The voltage control showed a fast response time by reaching reference value after 0.5 sec.

Fig. 5.15 shows the dc voltage when the filters were excluded. In the beginning when the voltage reference was set to be zero, then the controller was not able to track the reference.

But when the reference was set to 100 kV, then the outer controller was able to track the reference with good time response.

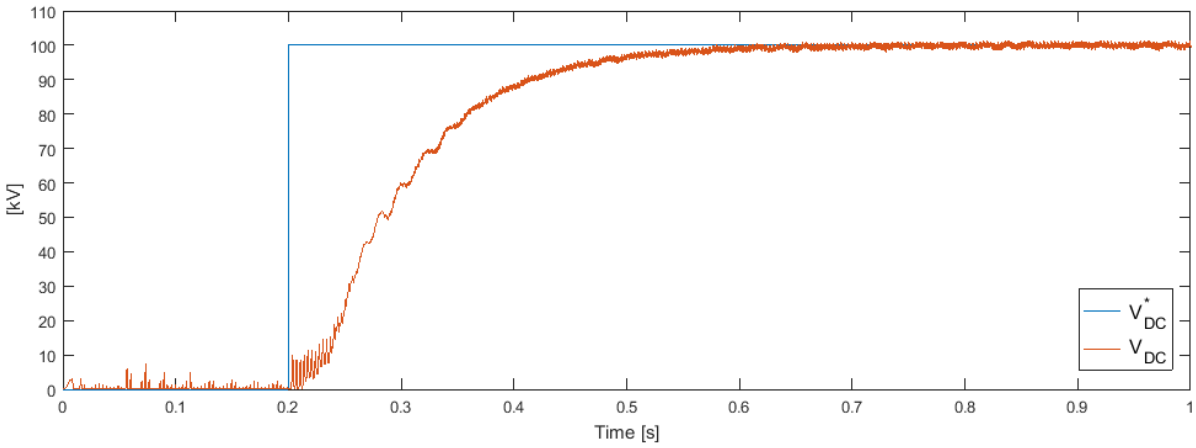

Figure 5.14: Balancing control when voltage reference is set to 100 kV after 0.2 sec.

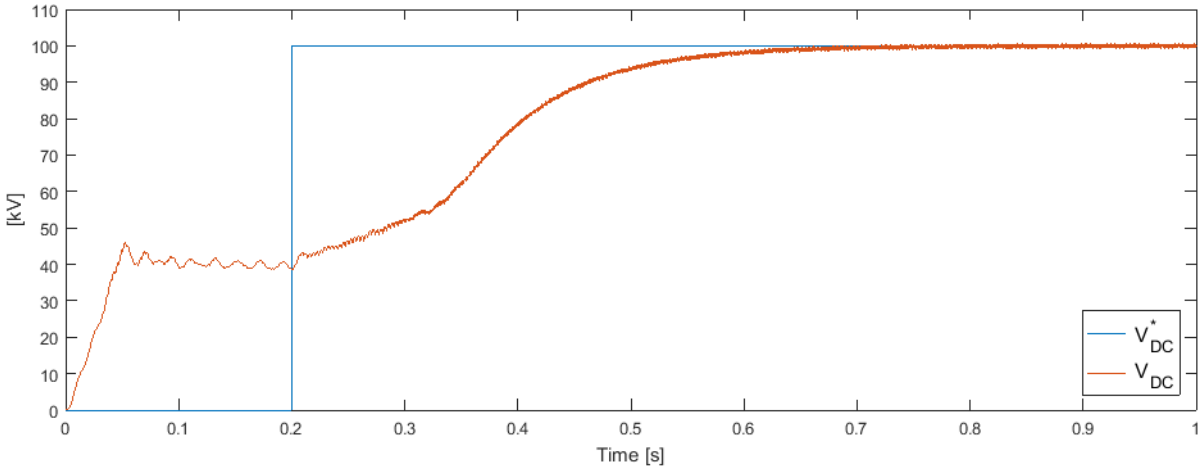

Figure 5.15: DC voltage when filters are excluded.

The other control objective was the harmonic control which eliminated the harmonic components in the source current. This control objective was fulfilled by applying a bank of BPF in the inner loop. The source current in $\alpha\beta$-coordinates from Fig. 5.16 shows how the reference was established when the dc reference value was set to 100 kV after 0.2 sec. The response time in the inner loop was observed to be faster than the outer loop because the current was able to track the reference after about 0.15 sec. This was one of the assumptions for utilizing a cascaded control loop.

The current was able to track the reference when the filters were included and properly tuned, and the 11th- and 13th- order harmonic components were almost neglectable as seen in Fig. 5.17. The importance of the harmonic filters can be observed in Fig. 5.18,

where the harmonic components are present. The THD of the source current was calculated to be equal to 1% when the filters were included, and equal to 3.4% when the filters were excluded. A THD equal to 1% is a good result and proves that the hybrid controller is able to eliminate all the harmonics in the grid.

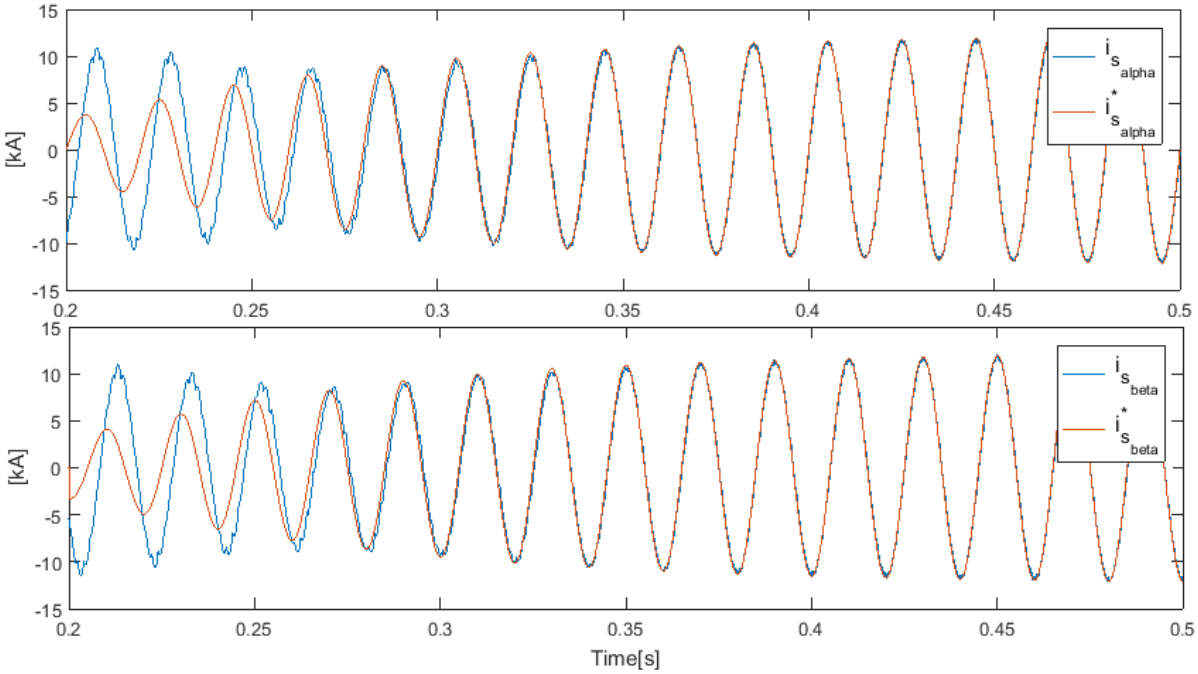

Figure 5.16: Harmonic control when voltage reference is set to 100 kV after 0.2 sec.

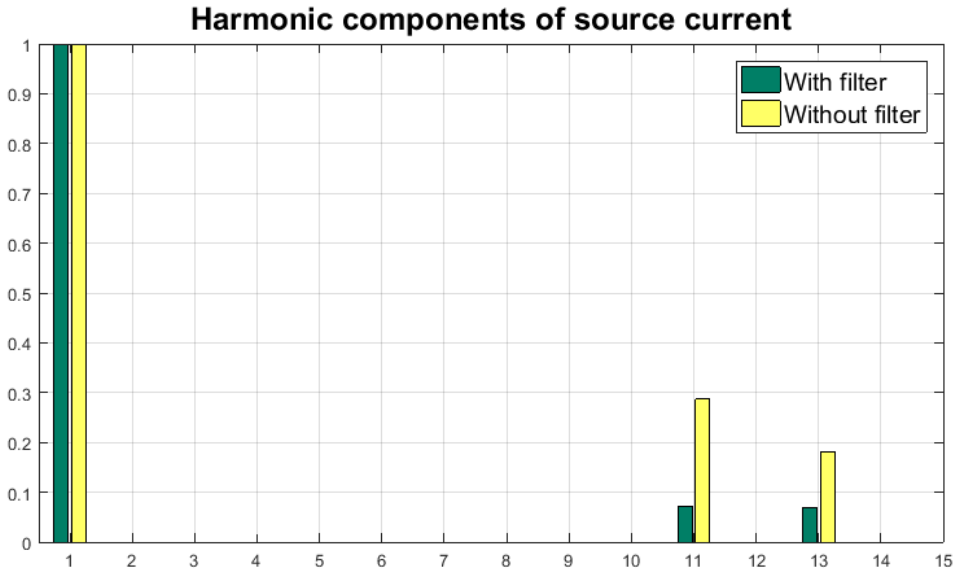

Figure 5.17: Harmonic spectrum of source current.

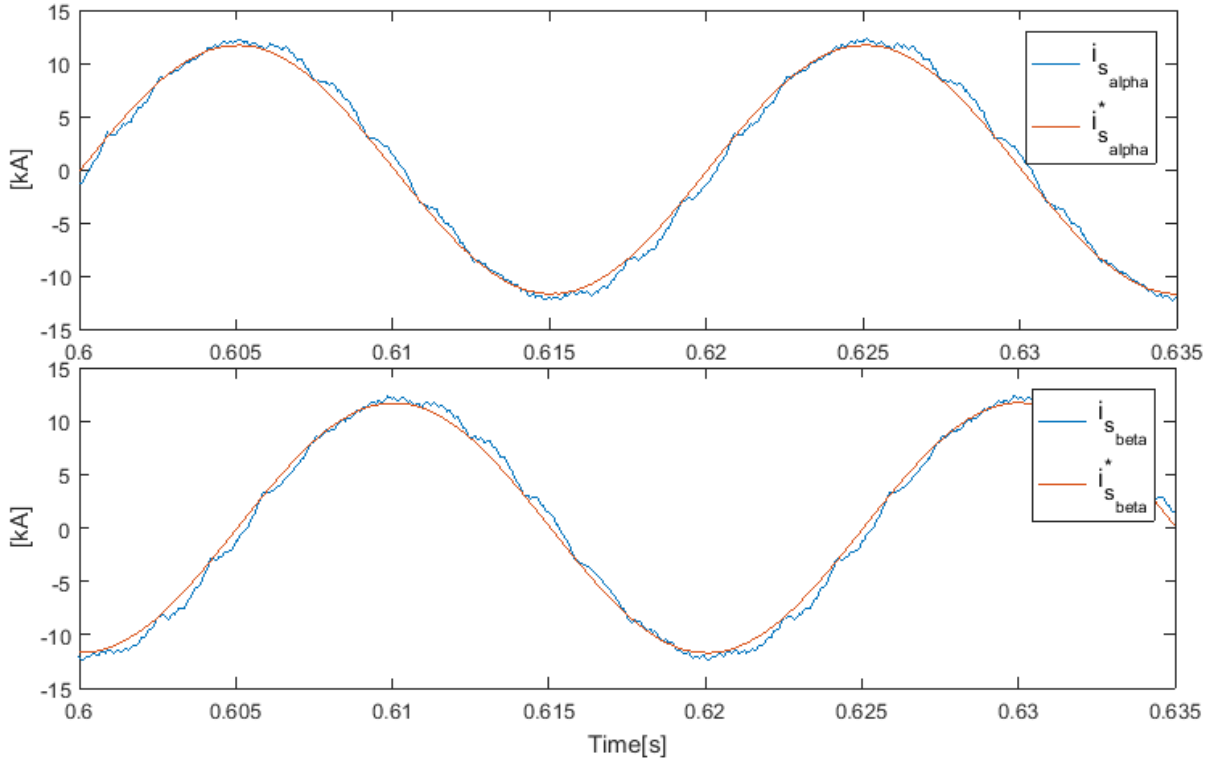

Figure 5.18: Source current in the $\alpha\beta$-reference plane when filters are excluded.

System Analysis

The whole system was analyzed because it was important to see how the hybrid topology operated. The active- and reactive power transfer, DC link voltage V_d and the series connected current i_d are shown in Fig. 5.19. The reference dc voltage was changed from 0 to 100 kV at t = 0.2 sec. It was observed that the power transfer from the WF doubled from 200 to 400 MW and that the DC link voltage was increased from 200 to 300 kV. In the beginning, before the controller was regulated, both the 12P-DR and the VSC were demanding reactive power equal to 300 MVAr in total. The WF had to provide the reactive power which is the reason why the active power transfer was limited.

The current i_p increased from 0.90 to 1.33 kA when the VSC started to control the dc voltage and to transfer active power. This current represents the power transferred through the VSC which was increased when the outer loop controller was regulated to a value larger than zero. It was experienced that the tuning of the outer loop PI controller was the most sensitive one. Without proper tuning, then the dc voltage was unstable and the whole system became unstable.

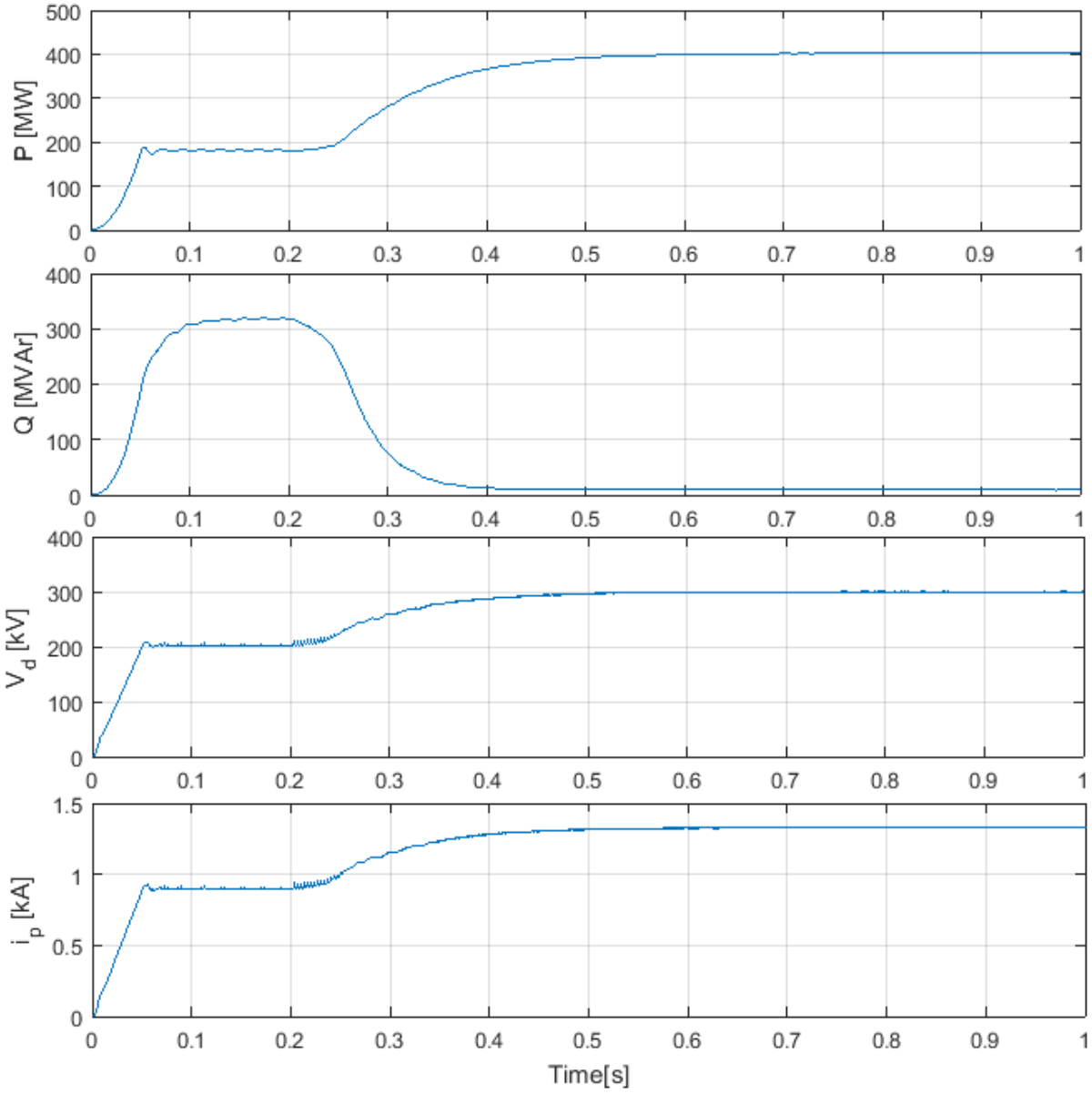

Figure 5.19: System operation (from the top): Active power flow from WF, reactive power flow from WF, DC link voltage, current in series connection between VSC and 12P-DR.

5.6 Discussion

The hybrid topology investigated in this thesis is an important contribution to the HVDC technology and it can improve the cost efficiency of offshore wind power transportation. Previously, in [12], a controller in the rotating reference frame for the hybrid DR-VSC topology was proposed. Now, in this thesis, a controller in the stationary reference frame has been proposed. The advantage of the $\alpha\beta$-frame is, as mentioned before, that it does not use a PLL, which is sensitive to harmonics in the offshore ac voltage. The PLL might be affected by the harmonics such that the VSC is not controlled properly.

In general, the topology has many advantages for OWF integration:

- Ability to control ac voltage, thus the WF will be able to control active power transfer.
- Power transfer in both directions results in black start capability.
- Passive filters are not needed because the VSC works as an APF.
- Fewer transistors are needed compared to a FRC, thus the system will be more robust, lower switching losses, and the price of power electronic devices will be reduced.

The topology is superior to the other two solutions presented in this thesis and to the VSC-HVDC topology. This is because it has more advantages than the other topologies. It is more robust, more efficient, and cheaper compared to the VSC-HVDC topology. Compared to the diode-based solutions will it be able to control ac voltage and it has black start capability. There is no need for an auxiliary power supply on the offshore converter station because of the black start capability, and maximum power can be obtained because the control objective of the FRC-WF does not need to be altered.

The drawback of the hybrid topology is the complexity of the controller, which is why an alternative topology was investigated in this chapter. The alternative topology took advantage of the FRC-WT's ability to alter its control objectives. The approach was called the APF approach because the APF controller was utilized with the same control parameters as in Ch. 4. By simulating the system with the less complex controller, it gave an indication of how the system will operate and that a controller based on the PBC approach was working. The drawback of this controller was that the voltage tracking control objective was not implemented. This resulted in potentially lost available power because the WF had

to control the ac voltage, thus it could not control the maximum power point tracker.

The simulation results for the single loop approach-controller showed that the controller was able to fulfill the voltage tracking control objective. It was also shown that the harmonic control objective remains to be fulfilled in future work, but the controller for an APF showed that it is possible to provide harmonic control with the PBC theory. The controller from the APF approach showed good performance; both harmonic components and reactive power were compensated and the outer loop showed a fast time response.

The hybrid DR-VSC topology presented in [12] has not been tested for frequency support, which is an important AS in future networks where there will be a high penetration of wind power. The hybrid topology should be tested for this service in future work, thus a chapter on frequency support can be found in Appendix C.

5.7 Summary

The hybrid DR-VSC topology has some advantages over VSC-HVDC topology which makes it an important field of research. Today, VSC-HVDC is the preferred technology for OWF integration, but it utilizes many transistors which are expensive, sensitive, and produce switching losses. The hybrid topology reduces the number of transistors needed, such that the converter station becomes cheaper, more robust, and has lower losses.

The research on control design of the DR-VSC hybrid has been a great challenge in this thesis. A sophisticated controller was researched and designed based on the model and the PBC theory. The controller has several control objectives which make it complicated, and these are voltage tracking control, harmonic control, and balancing control. The thesis lays the foundation for further work on this exciting new controller for the hybrid topology. A detailed plan for future work is given in the next chapter.

Also, a controller for a simplified model with less complex control objectives has been investigated in this chapter. The simplified system assumed that the WF was able to fulfill the voltage tracking objective such that the controller became less complex. Both harmonic- and balancing control was implemented for the hybrid topology and in the performance assessment, it was proved that the controller showed good performance. Both control objectives were fulfilled and the outer control loop showed fast time response, which is promising for future research.

Chapter 6

Summary and Recommendations for Future Work

6.1 Summary and Conclusion

Transmission of electricity to shore is one of the most important challenges in the offshore wind energy sector. It is challenging to avoid large losses and at the same time reduce the total cost. A VSC-based HVDC system is the preferred solution today because it is compact in size and has black start capability. **Alternative converter stations have been investigated and compared in this thesis** because the price and losses of the VSC should be reduced to optimize the transmission of offshore wind energy. A summary of the advantages and disadvantages discussed in the following subsections are presented in Table 6.1 in the end.

DR-Based HVDC Link

The topology which was presented first was the DR-based HVDC link, proposed by Blasco et al. in [9]. This topology took advantage of the FRC-WT, which could alter its control objectives such that it was able to control the offshore ac grid. The uncontrollable DRs could be used to convert the power because of this alteration. Even though there are benefits of utilizing uncontrollable diode rectifiers, like no switching losses, high robustness and cost savings in power electronic components, there are also some

disadvantages. These are the fact that bulky passive filters are required, maximum power is not controlled by the WF and an auxiliary power supply is needed for the start-up. The drawback with bulky passive filters is that they require a large converter platform which is both expensive and challenging to install at deep sea.

APF-DR HVDC Link

A solution which can reduce the size of the offshore platform is a similar solution where the passive filters are replaced by an APF. The APF is more compact than the passive filters and more flexible, but switching losses will be introduced. A quantitative study should be performed to investigate the size of the APF and the economic losses related to the power losses. The results should be compared to the solution proposed in [9] to see if it might be beneficial to install APFs at offshore platforms.

Hybrid DR-VSC HVDC Link

One of the objectives of this thesis was to **investigate a hybrid solution which could reduce the cost of the offshore platform**. A topology proposed by Nguyen et al. in [12] was investigated and compared to the other solutions. According to [12], would the topology improve the efficiency and have the same footprint as a VSC-HVDC link. Moreover, the cost of the converter station would be reduced because cheaper semiconductors could be used and because the price related to the footprint would be reduced. The advantages this topology had compared to the DR-APF solution was that the control objectives of the WF did not need to alter, such that maximum power point tracker could be controlled. Another advantage was that the VSC in series with the 12P-DR could transfer power in both directions, thus black start capability was ensured. All these advantages made the hybrid solution an interesting topology to investigate.

Table 6.1: Comparison table of the three converter solutions and a VSC-HVDC

	DR HVDC	**APF-DR HVDC**	**DR-VSC HVDC**	**VSC-HVDC**
Footprint[1]	Largest (large passive filters)	Medium (APF more compact than passive filters)	Small (same size as VSC-HVDC)	Small
Robustness	Highest (no switches)	Medium	Medium	Lowest (sensitive switches)
Losses	Lowest	Medium	Medium	Highest
Control objective	Not controllable	Easy	Complex	Easy
Black start capability	No	No	Yes	Yes
Alter control objectives of WF	Yes	Yes	No	No
Installation cost[2]	High (high installation cost because of large footprint)	Medium (smaller footprint)	Lowest (smallest footprint and cheaper power devices)	High (expensive transistors)

Control Design

Another objective of this thesis was to **design a control system for the hybrid converter station in the stationary reference frame**. This proved to be a challenging task because of the complex control objective. There were three objectives, harmonic control and balancing control which were similar to the APF control, and voltage tracking control. First, a controller for an APF, in stationary reference frame, were studied to develop an understanding of the passivity-based control design approach. This approach was later used to design a control system for the hybrid topology. First, a controller without balancing control was designed and the results showed that the controller was limited to linear loads. Because of time restrictions, it was decided to implement the APF-DR controller to show that the controller based on the PBC theory is able to work for harmonic loads. The APF-DR control objectives are less complex and it was observed that the controller was able to regulate a simplified system.

[1] Assumptions based on [9], [11] and [12].

[2] A quantitative study must be performed to prove these assumptions, which was outside the scope of this thesis.

Performance Assessment

A performance assessment was conducted to **investigate the control system behavior and the system dynamic performance** of the less complex controller for the hybrid topology. The controller showed a fast time response when initiated and it was observed that the controller was able to balance the dc voltage between the VSC and the 12P-DR. Moreover, the VSC was able to work as an active filter to eliminate the harmonic components in the source current and to compensate for the reactive power consumed by the 12P-DR.

Finally, it can be concluded that the hybrid topology has a complex controller which must be developed further, but the hybrid topology has the advantages of lower cost and losses which makes it an important solution for the future.

6.2 Future Work

An extensive research is still required to develop a controller for the hybrid topology and to find proofs that this is a superior solution. Here are some suggestions for future work:

- The single loop controller must be reformulated and implemented in PSCAD to prove that it is working for harmonic loads.
- Design controller with balancing control objective by calculating the conductance g-parameter in the same way as done for the APF.
- Find the optimal size of APF and VSC by calculating the reactive power consumed by the 12P-DR.
- Use a more precise tuning procedure for finding the control parameter values.
- Test system for frequency support by implementing torque control for the aggregated OWF. Connect the dc link to an onshore converter and a grid which can have a variable frequency. By adding an extra load, then the frequency will drop and the WF must be able to limit the frequency drop and to have a fast recovery to fulfill the Grid Codes. An introductory chapter on frequency support can be found in Appendix C.
- Perform a quantitative study which includes the real cost of equipment, installation, and maintenance for all the different solutions.

- Compare performance of the controller in the stationary reference frame and in the rotating reference frame.

Bibliography

[1] NASA. June 2017. URL: https://climate.nasa.gov/effects/.

[2] UNFCCC. Nov. 2016. URL: http://newsroom.unfccc.int/unfccc-newsroom/landmark-climate-change-agreement-to-enter-into-force/.

[3] I. Pineda and K. Ruby. *Wind in power: 2015 European statistics*. 2016.

[4] R. Adapa. "High-Wire Act: HVdc Technology: The State of the Art". In: *Power and Energy Magazine, IEEE* 10.6 (2012), pp. 18–29.

[5] Lie Xu and Bjarne R. Andersen. "Grid connection of large offshore wind farms using HVDC". In: *Wind Energy* 9.4 (2006), pp. 371–382.

[6] ABB. June 2017. URL: http://new.abb.com/systems/hvdc/why-hvdc/economic-and-environmental-advantages.

[7] Mike Barnes and Antony Beddard. "Voltage Source Converter HVDC Links – The State of the Art and Issues Going Forward". In: *Energy Procedia* 24 (2012), pp. 108–122.

[8] R. Blasco-Gimenez et al. "Variable voltage off-shore distribution network for wind farms based on synchronous generators". In: *20th International Conference and Exhibition on Electricity Distribution (CIRED)*. 2009.

[9] R. Blasco-Gimenez et al. "Distributed Voltage and Frequency Control of Offshore Wind Farms Connected With a Diode-Based HVdc Link". In: *IEEE Transactions on Power Electronics* 25.12 (2010), pp. 3095–3105.

[10] R. Blasco-Gimenez et al. "Diode-Based HVdc Link for the Connection of Large Offshore Wind Farms". In: *Energy Conversion, IEEE Transactions on* 26.2 (2011), pp. 615–626.

[11] A. Teke et al. "Active power filter: Review of converter topologies andcontrol strategies." In: *Gazi University Journal of Science*. Vol. 24. 2011, pp. 283–289.

[12] T. H. Nguyen, D. C. Lee, and Chan-Ki Kim. “A Series-Connected Topology of a Diode Rectifier and a Voltage-Source Converter for an HVDC Transmission System”. In: *Power Electronics, IEEE Transactions on* 29.4 (2014), pp. 1579–1584.

[13] T. H. Nguyen, D. C. Lee, and Chan-Ki Kim. “A cost-effective converter system for HVDC links integrated with offshore wind farms”. In: *IECON 2013 - 39th Annual Conference of the IEEE Industrial Electronics Society*. 2013, pp. 7978–7983.

[14] *Global Wind Report: Annual Market Update*. GWEC, 2016.

[15] ENTSO-E. “TSO Cooperation and the Internal Energy Market: Benefiting Consumers Across Europe”. In: *Annual Report*. 2013.

[16] Olimpo Anaya-Lara et al. *Wind Energy Generation : Modelling and Control*. Chicester: Wiley, 2009.

[17] E.On Netz. *Grid Code: High and extra high voltage*. GmbH, Bayreuth, 2006.

[18] Ned Mohan, Tore M. Undeland, and William P. Robbins. *Power electronics : converters, applications, and design*. 3rd ed. Hoboken, N.J: Wiley, 2003.

[19] ABB. *HVDC light: It’s time to connect*. 2012.

[20] Jos Arrillaga, Y. H. Liu, and Neville R. Watson. *Flexible Power Transmission : The HVDC Options*. Hoboken: Wiley, 2007.

[21] Karl M. Hink. “Harmonic Mitigation of 12-Pulse Drives with Unbalanced Input Line Voltages”. In: MTE Corporation.

[22] J. Arrillaga. *High voltage direct current transmission*. 2nd ed. Vol. 29. IEE power and energy series. London: Institution of Electrical Engineers, 1998.

[23] Chan-ki Kim. *HVDC transmission : power conversion applications in power systems*. Singapor: WileyBlackwell, 2009.

[24] Theodore R. Bosela. *Introduction to electrical power system technology*. Upper Saddle River, N.J: Prentice Hall, 1997.

[25] Edward Wilson Kimbark. *Direct Current Transmission*. New York: John Wiley, 1971.

[26] Marco Liserre, Frede Blaabjerg, and Antonio Dell’aquila. “Step-by-step design procedure for a grid-connected three-phase PWM voltage source converter”. In: *International Journal of Electronics* 91.8 (2004), pp. 445–460.

[27] L. Malesani et al. “AC/DC/AC PWM converter with reduced energy storage in the DC link”. In: *Industry Applications, IEEE Transactions on* 31.2 (1995), pp. 287–292.

[28] Elisabetta Tedeschi. “Lecture 13”. In: *ELK-23*. NTNU, 2016.

[29] M. Karimi-Ghartemani and M. R. Iravani. “A method for synchronization of power electronic converters in polluted and variable-frequency environments”. In: *Power Systems, IEEE Transactions on* 19.3 (2004), pp. 1263–1270.

[30] C. Schauder and H. Mehta. “Vector analysis and control of advanced static VAR compensators”. In: *IEE Proceedings C: Generation Transmission and Distribution* 140.4 (1993), pp. 299–306.

[31] Chandra Bajracharya. “Control of VSC-HVDC for wind power”. Thesis. 2008.

[32] Romeo Ortega et al. *Passivity-based Control of Euler-Lagrange Systems Mechanical, Electrical and Electromechanical Applications*. Springer London : Imprint: Springer, 1998.

[33] Hassan K. Khalil. *Nonlinear systems*. 2nd ed. Upper Saddle, N.J: Prentice Hall, 1996.

[34] “Basic Lyapunov theory”. In: *EE363 Lecture 12*. Stanford University, 2009.

[35] H. Akagi et al. “Generalized theory of the instantaneous reactive power in three-phase circuits”. In: *Proceedings of the International Power Electronics Conference* (1983), pp. 1375–1383.

[36] H. Akagi. “New trends in active filters for improving power quality”. In: *Proceedings of International Conference on Power Electronics, Drives and Energy Systems for Industrial Growth*. Vol. 1. Jan. 1996, 417–425 vol.1.

[37] G. Escobar, A. M. Stankovic, and P. Mattavelli. “An adaptive controller in stationary reference frame for D-statcom in unbalanced operation”. In: *IEEE Transactions on Industrial Electronics* 51.2 (2004), pp. 401–409.

[38] C. Bajracharya et al. “Understanding of Tuning Techniques of Converter Controllers for VSC-HVDC”. In: *Nordic Workshop on Power and Industrial Electronics*. Espoo, Finland, Helsinki University of Technology, 2008, pp. 1–8.

[39] R. Teodorescu and F. Blaabjerg. “Proportional-Resonant Controllers. A New Breed of Controllers Suitable for Grid-Connected Voltage-Source Converters”. In: *Proceedings of The 9th International Conference on Optimization of Electrical and Electronic Equipments*. 2004, pp. 9–14.

[40] A. Pietkiewicz and S. Melly. “Proper selection of passive and active power quality filters for the mitigation of mains harmonics”. In: *EE Times*. Schaffner EMV AG, 2008.

[41] Amirnaser Yazdani and Reza Iravani. *Voltage-Sourced Converters in Power Systems*. United States: John Wiley & Sons Inc, 2010.

[42] G. Escobar et al. “An Adaptive Control for UPS to Compensate Unbalance and Harmonic Distortion Using a Combined Capacitor/Load Current Sensing”. In: *Industrial Electronics, IEEE Transactions on* 54.2 (2007), pp. 839–847.

[43] P. Kundur. *Power system stability and control*. McGraw Hill, 1994.

[44] Machowski, Bialek, and Bumbi. *Power System Dynamic Stability and Control*. Wiley, 2008.

[45] Olimpo Anaya-Lara et al. *Offshore Wind Energy Generation : Control, Protection, and Integration to Electrical Systems*. Offshore Wind Energy Generation. Hoboken: Wiley, 2014.

[46] Anaya-Lara O. et al. “Intelligent control mechanisms for provision of virtual inertia”. In: *Integrated Research Program on Wind Energy (IRPWind)* (2017).

[47] J. Ekanayake and N. Jenkins. “Comparison of the response of doubly fed and fixed-speed induction generator wind turbines to changes in network frequency”. In: *Energy Conversion, IEEE Transactions on* 19.4 (2004), pp. 800–802.

[48] I.D. Margaris et al. “Frequency Control in Autonomous Power Systems With High Wind Power Penetration”. In: *IEEE Trans on Sustainable Energy* 3.2 (2012).

[49] Olimpo Anaya-Lara. “Synthetic inertia from wind generation”. In: *Marine Renewables Infrastructure Network* (2017).

[50] G. Ramtharan, J. B. Ekanayake, and N. Jenkins. “Frequency support from doubly fed induction generator wind turbines”. In: *IET Renewable Power* (2007), pp. 3–9.

Appendices

Appendix A

AC Filter Tuning

Different types of filters are applied to eliminate harmonic components in the current. The harmonics distort the sinusoidal shape and can be harmful to electrical equipment. Passive filters are connected in shunt to the diode-based converter solution presented in this thesis. The advantage of a shunt filter, in comparison to a series filter, is that it can provide reactive power and is relatively cheap [25]. Only a specific harmonic current will flow through the filter because the inductor and capacitor are tuned with a high-quality factor. Thus it only needs to be sized for a fraction of the total current, opposite to the series filter. The filter can be grounded at one end because it is connected in parallel, but a series filter must be isolated from the full voltage to ground which makes it more expensive. A higher quality factor gives sharper tuning of the filter, which results in almost complete elimination of the tuned low-order harmonic. The series RLC circuit, see Fig. A.1, can be applied in shunt at PCC and tuned to a specific frequency. The filter will then act as a low impedance branch for the specific harmonic component and lead it to ground such that the harmonic component will not affect the sinusoidal current at PCC.

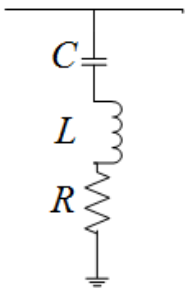

Figure A.1: Single-tuned shunt filter circuit.

The tuned angular frequency is defined in [25] and equal to

$$\omega_n = \frac{1}{\sqrt{LC}} = n * 2\pi f_F \tag{A.1}$$

where n is the specific harmonic component that must be eliminated (e.g. 5th, 7th, 11th or 13th) and f_F is the fundamental frequency. The inductor or capacitor reactance, when $\omega = \omega_n$, is defined as

$$X_0 = \omega_n L = \frac{1}{\omega_n C} = \sqrt{\frac{L}{C}} \tag{A.2}$$

$$Q = \frac{X_0}{R} \tag{A.3}$$

Q is the quality factor of the filter. By combining (A.1), (A.2) and (A.3), can the capacitor and inductor be calculated as

$$C = \frac{1}{\omega_n X_0} = \frac{1}{\omega_n RQ} \tag{A.4}$$

$$L = \frac{X_0}{\omega_n} = \frac{RQ}{\omega_n} \tag{A.5}$$

A typical value of the quality factor, Q, is between 0.5 and 5 for high-pass filters [22] Chap. 3.3.7. The risk of parallel resonance between filters and network increases with a larger value for Q, but it reduces the filter losses and harmonic voltage when correctly tuned [22].

Appendix B

Clark Transformation

A symmetrical ac system will provide a balanced ac voltage output equal to

$$\begin{bmatrix} V\cos\theta \\ V\cos(\theta - 2\pi/3) \\ V\cos(\theta - 4\pi/3) \end{bmatrix} \tag{B.1}$$

where V is the amplitude of the ac voltage in each phase and θ is the phase angle. The three-phased system in (B.1) is transformed into a two-phased $\alpha\beta$-coordinates in (B.2) by using the Clark-matrix from Table B.1.

Table B.1: Power invariant Clark transformation

Transformation	Transform	Matrix
Clark	from abc to $\alpha\beta$	$\sqrt{\frac{2}{3}} \cdot \begin{bmatrix} 1 & -\frac{1}{2} & -\frac{1}{2} \\ 0 & \frac{\sqrt{3}}{2} & -\frac{\sqrt{3}}{2} \end{bmatrix}$
Inverse Clark	from $\alpha\beta$ to abc	$\begin{bmatrix} 1 & 0 \\ -\frac{1}{2} & \frac{\sqrt{3}}{2} \\ -\frac{1}{2} & -\frac{\sqrt{3}}{2} \end{bmatrix}$

$$\sqrt{\frac{2}{3}} \cdot \begin{bmatrix} 1 & -\frac{1}{2} & -\frac{1}{2} \\ 0 & \frac{\sqrt{3}}{2} & -\frac{\sqrt{3}}{2} \end{bmatrix} \begin{bmatrix} V\cos\theta \\ V\cos(\theta - 2\pi/3) \\ V\cos(\theta - 4\pi/3) \end{bmatrix} = \begin{bmatrix} V\cos\theta \\ V\sin\theta \end{bmatrix} \tag{B.2}$$

Appendix C

Frequency Support

C.1 Introduction

The provision of frequency support is especially important for providing system stability. Frequency is a stability measure which indicates if the consumption exceeds the production with a drop in frequency and vice versa. It is stated in the Grid Codes that generation plants need to deliver frequency support as an AS if the frequency drop exceeds the statutory limits [17].

Primary power control is a challenge for the OWF when it is decoupled from the network by submarine dc cables. A drop in frequency will not automatically be noticed by the offshore wind farm because of the electrical converters. This is different from conventional power plants where the generator will immediately slow down and release kinetic energy to deliver more power in case of a drop in frequency.

Communication between the generator and the onshore grid is necessary for the generator to detect any faults in the grid; in voltage or in frequency dips. When communication is established, a change in frequency will be detected by the generators. For the provision of frequency support, it is important that the OWF is fitted with suitable controls.

To explain the concept of frequency support this section will start with an explanation of the natural responses in frequency, then the provision of frequency support from conventional power plants will be explained, and finally different control strategies for the OWF will be presented.

C.2 Dynamic Frequency Response

The system frequency is dependent on active power balance. If there is a change in active power demand at any point in the system it will reflect in the frequency throughout the system [43]. A sudden increase in load or loss of generation will give a mismatch between generation and supply and as a result, there will be a change in the system frequency. The dynamic response in frequency can be divided into four parts depending on the duration of the dynamics involved [44] Ch. 9.2:

- Part 1: Rotor swings in the generators (first few seconds)
- Part 2: Frequency drop (a few seconds to several seconds)
- Part 3: Primary control by the turbine governing system (several seconds)
- Part 4: Secondary control by the central regulators (several seconds to minutes)

There are two important dynamic responses, rotor swings, and frequency drop. They occur in the first seconds after a sudden change in demand or production. The generating power plant will provide frequency support in two parts, namely primary and secondary power control, when it notices a change in frequency. Primary power control is provided by an automatic droop control loop and generators increase their power output depending on the time lag of the prime mover and the dead band of the governor [16]. Secondary control brings the frequency back to the nominal value by utilizing a slow supplementary control loop [44]. Fig. C.1 shows a typical frequency response in England and Wales. Stage 1 and stage 2 occurs in the first few seconds which is marked by “event” in the figure. Primary and secondary control is marked as the primary and secondary response.

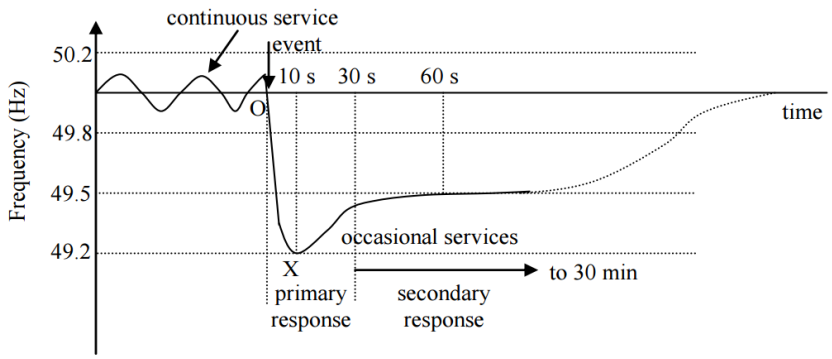

Figure C.1: Frequency drop and provision of frequency support [16].

Part 1 - Rotor Swings

Rotor swings are the dynamic response immediately after a change in load or generation. If a load is connected to the system then the equivalent impedance x_t of the system will decrease, and consequently, the electrical power P_e of the system increases as seen by (C.1) given in [44] Ch. 9.2:

$$P_e = \frac{EVs}{X_t} \sin\delta \tag{C.1}$$

where E is the transient emf behind an equivalent reactance X_t, V_s is the system voltage and δ is the power angle.

The rotor angle of the generator is not able to change immediately, thus there will be an imbalance between electrical and mechanical power P_m [44]

$$P_a = P_m - P_e$$

where P_a is the power needed to balance the system. The power imbalance is also described by the swing equation (C.4) which is derived in subsection C.3. The power imbalance will only last for a few seconds before the frequency drops.

Part 2 - Frequency Drop

The imbalance in the power system, resulting from a higher power demand than generated power, will make the generators in the system slow down and the frequency to drop [44] Ch. 9.3. The rate of frequency drop is dependent on the system inertia, which is the sum of inertia for each connected generator. The system inertia is the ability to resist any change of motion. If the inertia is low, then the frequency will drop to low values before the generators are able to actively control the output power.

C.3 Frequency Control in Conventional Power Plants

Synchronous Generator Characteristics

When there is an unbalance in the system power, there will be an accelerating torque

$$T_a = T - m - T_e$$

where T_m and T_e are the mechanical and electrical torque respectively. The swing equation, i.e. equation of motion, can be found in [43] as

$$J\frac{d\omega}{dt} = T_a = T_m - T_e \tag{C.2}$$

where ω is the rotor speed and J is the effective inertia of the rotating components. The swing equation can also be written using the inertia constant H, which is defined as

$$H = \frac{1}{2}\frac{j\omega_0^2}{S} \tag{C.3}$$

where ω_0 is the rated speed and S is the rated power of the electrical machine. Combining (C.2) and (C.3) gives the per unit swing equation

$$2H\frac{d\overline{\omega}}{dt} = \overline{T_m} - \overline{T_e} \tag{C.4}$$

where the notation $\overline{(.)}$ stands for per unit.

A load change in the system is instantaneously reflected as a change in electrical torque T_e, and the unbalance between T_m and T_e results in speed variations as determined by (C.4). The generators will slow down and the frequency will drop as described in the previous section.

Primary Power Control

Primary power control is the first action performed to limit the frequency drop. It is provided by the speed governor of each generating unit and the principle is illustrated in

Fig. C.2, where a generating unit supplies a local load.

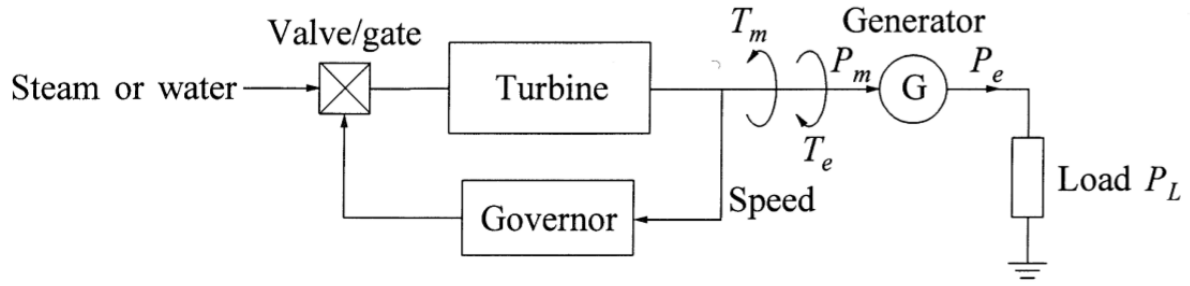

Figure C.2: Generator supplying local load [43].

Equation (C.4) explains the same principle as Fig. C.2, which is that an unbalance in the system power will result in a frequency change/speed change. The change of speed in the rotor is measured by the governor and compared with a reference. A governor controller is presented in Fig. C.3 where a steady-state feedback loop, R, is added around the integrator. δ Y is the control signal which actuates the valve/gate for the steam/water-supply in the conventional power plant.

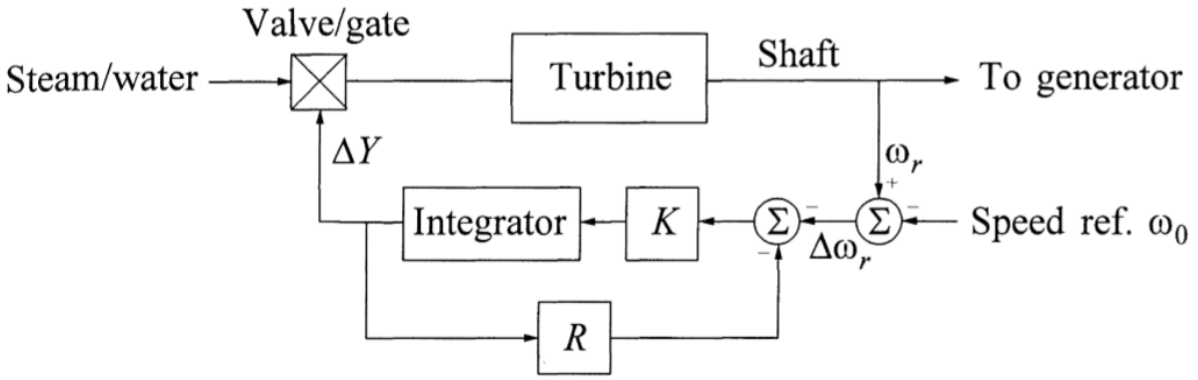

Figure C.3: Governor with steady-state feedback loop [43].

For multiple generating units connected to the same system, it is necessary with a coordinated regulation. The governors are provided with a speed-droop characteristic to provide the regulation [43]. The parameter R is the droop constant or speed regulation and is defined as the change of frequency over the change in power output:

$$R = \frac{f - f_0}{\Delta P}$$

where f_0 is the rated frequency of the system. The parameter R is controlled to give a specific droop characteristic which gives the desired rate of frequency change.

C.4 Frequency Control in Wind Farms

Synthetic Inertia

In conventional power plants will the rotor sense the frequency change and the governor will set a new reference for the output power. When the wind turbine generator is decoupled from the grid, it will not be able to detect a frequency change and therefore a frequency change must be communicated to the OFW. When communication is established then the frequency response must be provided by an additional control loop of the output power. The control of output power will emulate the inertial response of a conventional generator and is therefore called synthetic inertia or fast primary response [45]. Providing synthetic inertia is essential in the frequency control from a wind turbine, and will be a future demand in the grid codes.

Control Strategy

The focus for wind power contribution to system inertia are the provision of primary control (frequency response) and provision of synthetic inertia (fast primary response) [46]. Another widely accepted control strategy is the de-loading technique, which will be explained briefly in this subsection together with two control strategies utilizing the kinetic energy stored in the rotating masses.

De-loading of wind turbines for frequency support involves a de-load of the maximum power extraction curve to keep a certain power reserve. The power reserve can be used to accelerate the generator when the system frequency drops. A blade pitch angle controlled wind turbine in [47], is utilizing an additional control loop in the turbine torque control for decelerating the generator speed. The drawback with this method is the lost energy in normal operation when the generator is forced to operate with a power reserve.

Droop control is an approach described in subsection C.3 for conventional power plants and was called primary power control. The basic idea is to control the power output by utilizing some of the stored kinetic energy in the rotor. A droop constant, which is the relation between the frequency change and the accelerating power, is controlled to give the desired droop characteristic. Droop control together with inertial control is the most used

approach for frequency support in variable speed wind turbines [46]. Inertia control is applied to each individual wind turbine and droop control is implemented in the central control for the whole wind farm [48].

Inertial control is provided by the wind turbine and can be obtained by controlling the power output with an additional control loop. By controlling the output power in response to frequency changes, then the turbine can appear as a conventional power plant with synchronously connected inertia [49]. There are different approaches for providing inertial control, but generally, it involves modifications of the turbine torque/speed controller.

An approach described in [49] calculates the demanded torque which is needed to provide the synthetic inertia. The demanded torque T_d is calculated by introducing $T_{inertia}$, which is the torque corresponding to the frequency change

$$T_d = T_{ref} + T_{inertia}$$

where T_{ref} is the torque needed in normal operations. The schematic of the controller is shown in Fig. C.4 and sets the reference for the turbine wind farm controller.

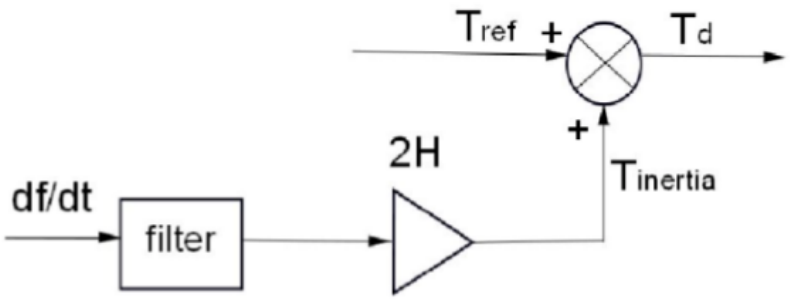

Figure C.4: Inertial control by introducing $T_{inertia}$ [49].

T_{ref} is determined from the rotor characteristic curve for maximum power extraction as seen in Fig. C.5 [50]. The figure also shows the supplementary control loop similar to Fig. C.4, which calculates the influence of the frequency change to set a new reference for the demanded torque.

The disadvantage with inertial control is that it can be difficult to recover the rotor speed after a deceleration of the machine rotor, which is why it can be favorable to combine the different control methods. In a collaborative project called Integrated Research Program on Wind Energy (IRPWind), all three control strategies explained in this section are assembled

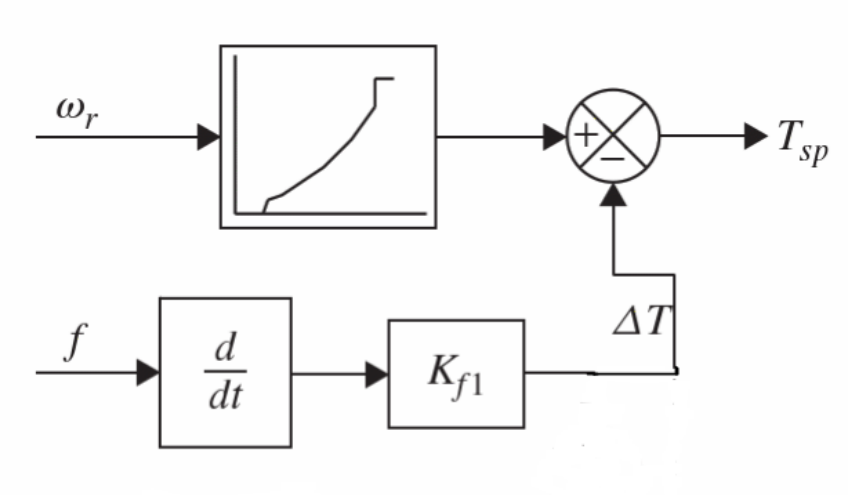

Figure C.5: Supplementary control loop for machine inertia [16], [50].

together to set the power reference [46]. The controller is able to stabilize the system in case of a frequency drop when the level of wind energy in the system is 20%. For higher wind penetration, the necessity of power reserves is essential.